

MIT Open Access Articles

The nature of transition from adakitite to non-adakitite magmatism in a slab window setting: A synthesis from the eastern Pontides, NE Turkey

The MIT Faculty has made this article openly available. **Please share** how this access benefits you. Your story matters.

Citation: Eyuboglu, Yener, M. Santosh, Francis O. Dudas, Enver Akaryali, Sun-Lin Chung, Kemal Akdag, and Osman Bektaş. "The Nature of Transition from Adakitite to Non-Adakitite Magmatism in a Slab Window Setting: A Synthesis from the Eastern Pontides, NE Turkey." *Geoscience Frontiers* 4, no. 4 (July 2013): 353–375. © 2012 China University of Geosciences (Beijing) and Peking University

As Published: <http://dx.doi.org/10.1016/j.gsf.2012.10.001>

Publisher: Elsevier

Persistent URL: <http://hdl.handle.net/1721.1/90629>

Version: Final published version: final published article, as it appeared in a journal, conference proceedings, or other formally published context

Terms of use: Creative Commons Attribution



Contents lists available at [SciVerse ScienceDirect](#)

China University of Geosciences (Beijing)

Geoscience Frontiers

journal homepage: www.elsevier.com/locate/gsf

Research paper

The nature of transition from adakitic to non-adakitic magmatism in a slab window setting: A synthesis from the eastern Pontides, NE Turkey



Yener Eyuboglu^{a,*}, M. Santosh^b, Francis O. Dudas^c, Enver Akaryalı^d, Sun-Lin Chung^e, Kemal Akdağ^a, Osman Bektaş^a

^a Department of Geological Engineering, Karadeniz Technical University, 61080 Trabzon, Turkey

^b School of Earth Sciences and Resources, China University of Geosciences (Beijing), 29 Xueyuan Road, Beijing 100083, China

^c Department of Earth, Atmospheric and Planetary Sciences, Massachusetts Institute of Technology, Cambridge, MA 02139, USA

^d Department of Geological Engineering, Gumushane University, 29000 Gumushane, Turkey

^e Department of Geosciences, National Taiwan University, Taipei 10617, Taiwan

ARTICLE INFO

Article history:

Received 1 August 2012

Received in revised form

9 October 2012

Accepted 19 October 2012

Available online 12 November 2012

Keywords:

Adakite

Geochemistry

Zircon U–Pb geochronology

Magma tectonics

Eastern Pontides

ABSTRACT

The eastern Pontides orogenic belt provides a window into continental arc magmatism in the Alpine–Himalayan belt. The late Mesozoic–Cenozoic geodynamic evolution of this belt remains controversial. Here we focus on the nature of the transition from the adakitic to non-adakitic magmatism in the Kale area of Gumushane region in NE Turkey where this transition is best preserved. The adakitic lithologies comprise porphyries and hyaloclastites. The porphyries are represented by biotite-rich andesites, hornblende-rich andesite and dacite. The hyaloclastites represent the final stage of adakitic activity and they were generated by eruption/intrusion of adakitic andesitic magma into soft carbonate mud. The non-adakitic lithologies include basaltic-andesitic volcanic and associated pyroclastic rocks. Both rock groups are cutting by basaltic dikes representing the final stage of the Cenozoic magmatism in the study area. We report zircon U–Pb ages of 48.71 ± 0.74 Ma for the adakitic rocks, and 44.68 ± 0.84 Ma for the non-adakitic type, suggesting that there is no significant time gap during the transition from adakitic to non-adakitic magmatism. We evaluate the origin, magma processes and tectonic setting of the magmatism in the southern part of the eastern Pontides orogenic belt. Our results have important bearing on the late Mesozoic–Cenozoic geodynamic evolution of the eastern Mediterranean region.

© 2012, China University of Geosciences (Beijing) and Peking University. Production and hosting by Elsevier B.V. All rights reserved.

1. Introduction

Continental arcs are potential sites of magmatism and tectonism in convergent margins (e.g., [Casquet et al., 2012](#); [Condie and Kröner, 2012](#)). The eastern Pontides orogenic belt provides one of the well-preserved examples of continental arcs in the Alpine–Himalayan

belt. However, its late Mesozoic–Cenozoic geodynamic evolution remains controversial due to lack of systematic geological, geochemical and geochronological data. Several workers suggested that this belt was shaped by the northward subduction of an oceanic lithosphere (Paleotethys or Neotethys) in the late Mesozoic and following the collision between Pontide and Tauride blocks in the south of the arc during Paleocene (e.g., [Adamia et al., 1977](#); [Şengör and Yılmaz, 1981](#); [Ustaömer and Robertson, 1996](#); [Okay and Şahintürk, 1997](#); [Arslan and Aslan, 2006](#); [Dilek et al., 2010](#); [Topuz et al., 2011](#)). In contrast, [Dewey et al. \(1973\)](#), [Bektaş et al. \(1999\)](#), [Eyuboglu \(2010\)](#) and [Eyuboglu et al. \(2011a,b,c,d,e\)](#) proposed a southward subduction model for the late Mesozoic–Cenozoic geodynamic evolution of the region, based on paleomagnetic, tectonic and magmatic records. According to this model, the Black Sea and Caspian Sea are the remnants of an ancient ocean (Paleotethys).

* Corresponding author.

E-mail address: y_eyuboglu@hotmail.com (Y. Eyuboglu).

Peer-review under responsibility of China University of Geosciences (Beijing)



Production and hosting by Elsevier

The late Mesozoic–early Cenozoic magmatism is represented by five main cycles: shoshonitic (early Campanian), ultrapotassic (Maastrichtian–early Paleocene?), adakitic (late Paleocene–early Eocene), non-adakitic basaltic-andesitic magmatism (early to middle Eocene) and non-adakitic granitic intrusions (Eocene) in the southern part of the eastern Pontides orogenic belt (Eyuboglu, 2010; Eyuboglu et al., 2011a,b,c,d,e). In a previous study, we proposed that the transition from shoshonitic to ultrapotassic magmatism is related to steepening of the southward subducting Tethys oceanic lithosphere during the Maastrichtian–early Paleocene (Eyuboglu et al., 2011a). The ultrapotassic magmatism was followed by intense adakitic activity (Cycle 3). However, debate continues regarding the origin of the adakitic magmatism and its geodynamic setting. According to some authors (Dilek et al., 2010; Karsli et al., 2010; Topuz et al., 2011), the eastern Pontides late Paleocene–early Eocene adakitic rocks formed by partial melting of thickened or delaminated lower continental crust after the collision between Pontides and Taurides to the south of the eastern Pontides magmatic arc during Paleocene. In a different model, Eyuboglu et al. (2011a,b,c,d,e) suggested that the adakitic rocks were generated by slab window-related processes during the ridge subduction in a south-dipping subduction zone. The fourth cycle of the magmatism includes non-adakitic basaltic-andesitic volcanic and associated pyroclastic rocks of middle Eocene.

In this study, we focus on the nature of the transition from the adakitic (Cycle 3) to non-adakitic magmatism (Cycle 4) in the Kale area (Gumushane, NE Turkey), which is one of the classic localities to evaluate this transition. In addition, we present new field data, zircon U–Pb geochronology and whole rock geochemistry in order to understand the origin and tectonic setting of the adakitic and non-adakitic early Cenozoic magmatism in the southern part of the eastern

Pontides orogenic belt. We also discuss the late Mesozoic–Cenozoic geodynamic evolution of the eastern Mediterranean region in the light of the new data.

2. Geological background

The eastern Pontides orogenic belt geographically corresponds to the eastern Black Sea region of Turkey and occurs within the Alpine metallogenic belt. The belt is approximately 500 km long and 200 km wide and has been divided into Northern, Southern and Axial subzones (Bektaş et al., 1995; Eyuboglu et al., 2006). Each of these zones is separated by E–W-, NE–SW- and NW–SE-trending faults, thus attributing a block-faulted structural architecture for the entire belt (Bektaş and Çapkinoglu, 1997; Eyuboglu et al., 2006, 2007). The Northern Zone is dominantly composed of Mesozoic–Cenozoic volcanic rocks, associated with massive-sulfide deposits and calderas, together with granitic intrusions (Fig. 1). The Southern Zone is generally represented by Mesozoic and Eocene sedimentary rocks, adakitic and shoshonitic magmatic rocks, pre-Liasic ultramafic-mafic cumulates, and metamorphic-granitic rocks belonging to the Hercynian basement (Pulur, Ağvanis and Tokat metamorphic massifs, Kurtoğlu and Karadağ metamorphic units, Köse and Gümüşhane granitoids). Upper mantle peridotites (?) and a middle to upper Cretaceous olistostromal mélange occur extensively farther south in the Axial Zone.

The Gumushane area is located in the southern zone of the eastern Pontides orogenic belt (Fig. 1). The pre-Jurassic basement here is represented by the Kurtoğlu metamorphics and unmetamorphosed Gümüşhane and Köse Granitoids. The Kurtoğlu metamorphics extend as a narrow ribbon along the southern border of the late Carboniferous Gümüşhane pluton and comprise mainly mica

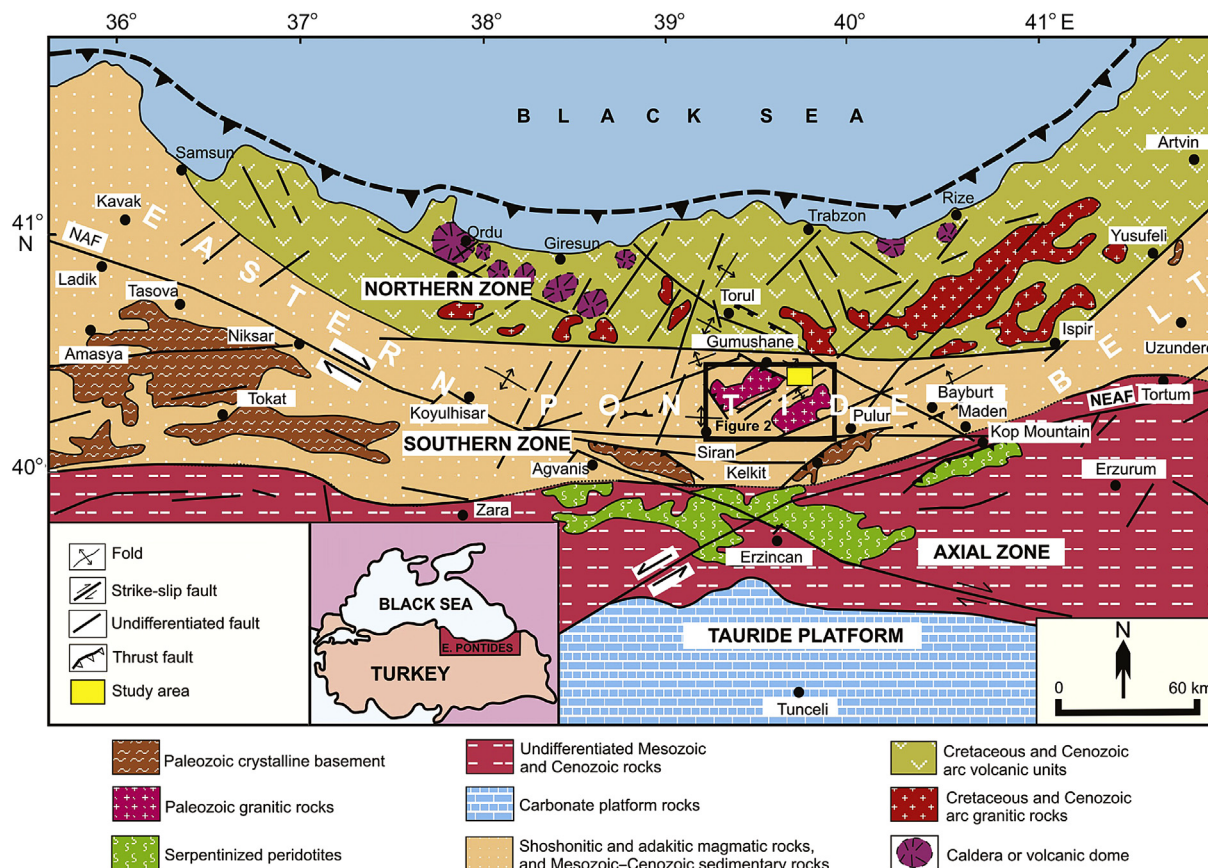


Figure 1. Main lithological units and tectonic zones of the eastern Pontides orogenic belt. NAF: North Anatolian Fault; NEAF: Northeast Anatolian Fault (after Eyuboglu et al., 2006).

schists, gneisses and phyllites, cut by metagranitic dikes (Fig. 2). Similar lithologies, albeit on a small scale, also appear around the Melike valley and the Beyçam village at the northeast extension of the main body (Fig. 2). The minimum age for the metamorphic event in this unit is Carboniferous, dated as 320.3 ± 1.7 Ma (Topuz et al., 2007). This metamorphic unit is intruded by the late Carboniferous Gümüşhane and Köse granitoids including various rock types such as granite, granodiorite, quartz diorite, rhyolite, and dacite (Topuz et al., 2010; Dokuz, 2011). These plutons are extensively cut by basic dikes of unknown age but are texturally similar to early-mid-Jurassic magmatic units in the region. The pre-Jurassic basement rocks are transgressively overlain by early and middle Jurassic Zimonköy Formation (Figs. 2 and 3), which is widely distributed in the eastern Pontides, from Amasya in the west to Artvin in the east. The detailed field studies on this formation showed that there were two main rifting phases during Jurassic (Eyuboglu et al., 2006). The first phase is characterized by asymmetrical half grabens and accumulation of volcanics and associated coarse clastics. However, during and subsequent to the first rifting, the rift-related basins experienced short-term thermal subsidence resulting in the deposition of pelagic limestones of Ammonitico-Rosso. The second rifting of the Jurassic began with second sequence of alternating volcanics and epiclastics (Eyuboglu et al., 2006). This rift-related sequence is overlain by the late Jurassic to early Cretaceous carbonates (Berdiga Formation) during long-lived thermal subsidence in the entire eastern Pontides (Fig. 3). The late Cretaceous is characterized by a thick sedimentary sequence in the Gumushane area. This unit known as the Kermutdere Formation starts with yellowish sandy limestones on the

carbonate platform and grades upward into red pelagic limestones and continues with sandstone, siltstone, claystone, marl and limestone alternation, with locally interbedded tuff. However, in the southeastern part of the study area (Fig. 3), poorly sorted monogenic conglomerate occurs extensively, composed of late Jurassic–early Cretaceous limestone fragments, constituting the lower part of the Kermutdere Formation. This conglomerate might have been derived from the uplifted limestone ridges related to block-faulting tectonics and/or sea-level changes before the deposition of the Kermutdere Formation. On the other hand, the late Cretaceous is represented by bimodal volcanic rocks and arc-related I-type granitic intrusions about 35 km northwest of the study area (Kaygusuz et al., 2008). These autochthonous Paleozoic and Mesozoic units are intruded by porphyry andesites and dacites (Figs. 3 and 4A, B, D), which are among the main topics in this study. The whole sequence is unconformably overlain by the early Cenozoic Alibaba Formation including basal conglomerate (Fig. 4C), nummulite-bearing limestone, and a thick volcanic sequence consisting mainly of basalt-andesite and associated pyroclastic rocks and intruded by the late Eocene granitic intrusions (Arslan and Aliyazıcıoğlu, 2001; Arslan and Aslan, 2006; Eyuboglu et al., 2011a). All of these units are cut by basic dikes representing the final stage of the Cenozoic magmatism (Fig. 4E and F).

3. Field geology and petrography

In the Kale area (Gumushane), the Cenozoic magmatic rocks can be divided into two main groups as adakitic and non-adakitic.

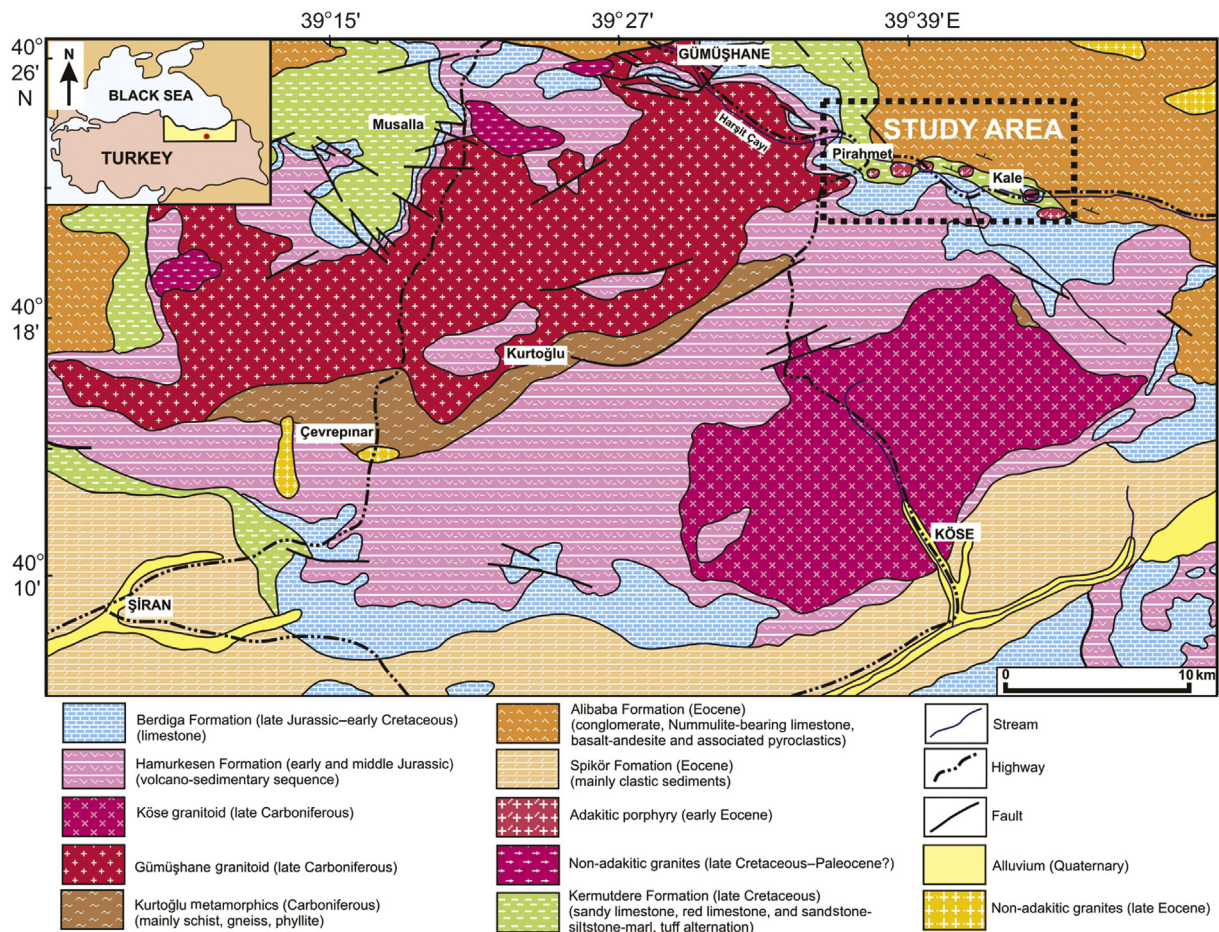


Figure 2. Geological map of the southern part of the Gumushane region (after Güven, 1993).

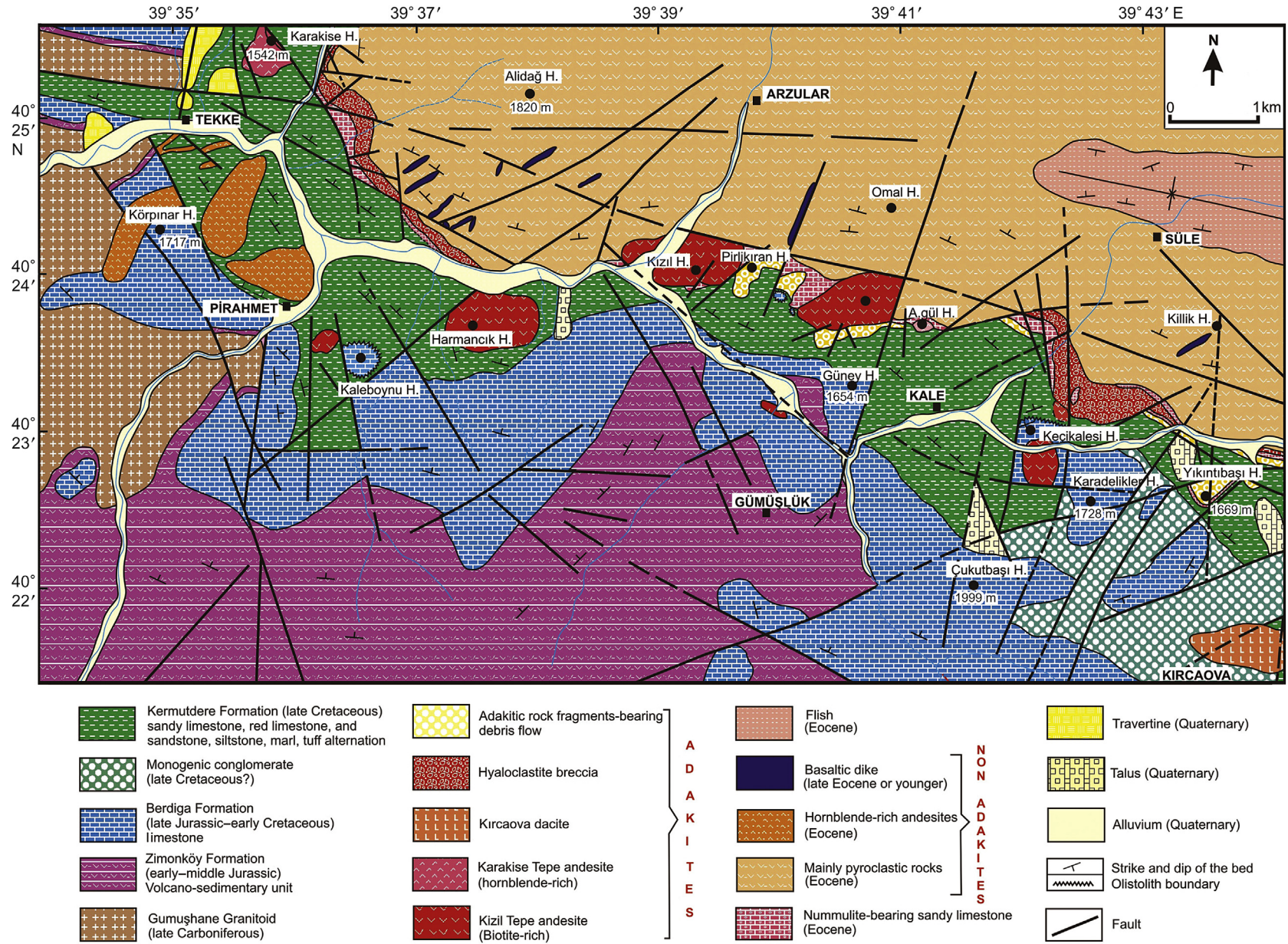


Figure 3. Geological map of the Kale area, showing the distributions and stratigraphic relations of the studied rocks and also main tectonic lines.

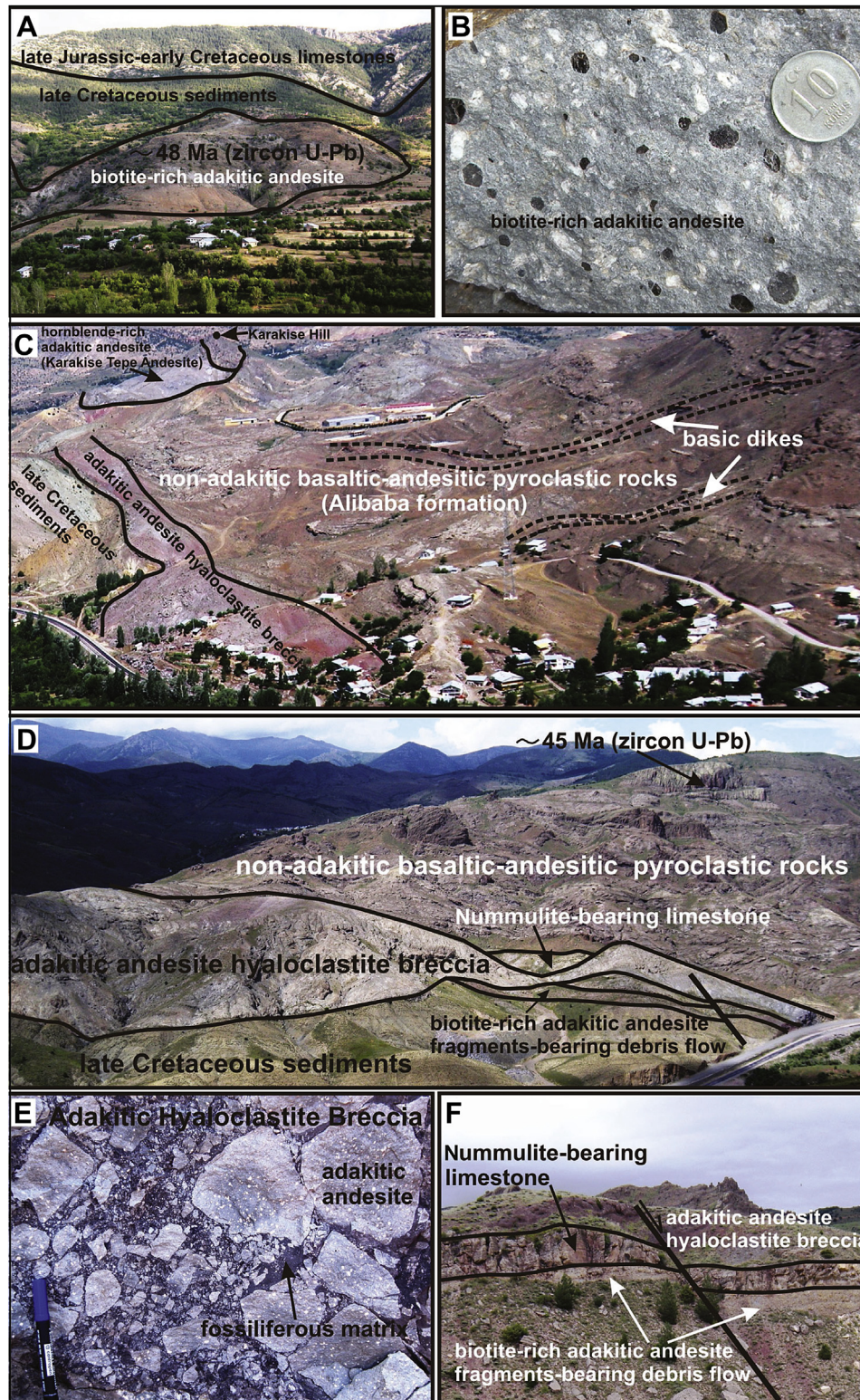


Figure 4. Representative field photographs, showing the field characteristics and contact relations of the studied adakitic and non-adakitic rocks. (A) A biotite-rich adakitic intrusion cutting the late Cretaceous Kermutdere formation at the immediately south of Harmancık village, (B) Large biotite crystals in the hand specimen taken from Kızıl Tepe andesite, (C) Basaltic dikes cutting the Eocene Alibaba formation, (D) The contact relations between adakitic and non-adakitic lithologies at the immediately west of Keçikalesi Hill, (E) Andesite fragments in adakitic hyaloclastite breccia, (F) Transition from adakitic to non-adakitic magmatism in the north of Kale village.

3.1. Adakitic rocks

The adakitic intrusions exposed in the Kale (Gumushane) area are hosted by pre-middle Eocene autochthonous units such as the

early to mid-Jurassic Zimonköy Formation, the late Jurassic to early Cretaceous Berdiga Formation and the late Cretaceous Kermutdere Formation. The distribution of mappable bodies, which are well-exposed along about NW–SE-trending line, is concordant with the

regional structural grain of the eastern Pontides (Figs. 1 and 3). Their size ranges from less than 0.1–2 km², and the outcrop patterns vary from round or elliptical to markedly elongate. In addition to these intrusive bodies, a hyaloclastite breccia horizon, which includes angular fragments of the hornblende-rich adakitic andesites, rests upon or occurs within the basement units of Eocene sequence and also upon the late Cretaceous Kermutdere Formation in the some locations (Fig. 3). All the adakitic units and their host rocks are unconformably overlain by volcanic assemblages of the early Cenozoic Alibaba Formation (Fig. 4).

The adakitic rocks exposed in the Gumushane area, based on field and petrographic characteristics, can be divided into four subgroups: (i) biotite-rich porphyritic quartz andesite (Kiziltepe andesite); (ii) hornblende-rich porphyritic andesite (Karakisetepes andesite); (iii) dacite (Kircaova dacite); and (iv) andesitic hyaloclastite breccia.

3.1.1. Biotite-rich porphyritic quartz andesite (Kizil Tepe andesite)

The main outcrops of the biotite-rich porphyritic quartz andesite, which was first recognized by Eren (1983) as 'Harmançiktepe dacite', occur as small, ellipsoidal bodies around Harmançik Hill, Kızıl Hill and an unnamed hill located at the central part of the map area (Figs. 3 and 4A, B). In addition, very small bodies of this group are exposed around Murathanoglu village and Keci-kale Hill and immediately west of the Kaleboynu Hill (Fig. 3). All of these bodies show sharp contact with their host rocks. The rock is characterized by abundant euhedral to subhedral biotite crystals in hand specimen (Fig. 4B). Fresh surfaces are light to medium gray in color (Fig. 4B). On weathered surfaces, the rock is characteristically whitish gray, brownish or buff colored. In thin section, the rock is a porphyritic andesite, slightly clay-rich, oxidized and contains domains consisting of partly recrystallized aggregates of spherulite. The phenocrysts/glomerocrysts are predominantly zoned plagioclase, hornblende, biotite and a few subrounded and broken fragments of quartz. The biotite phenocrysts are deformed and partly replaced by chlorite and clays along the cleavage traces. Some are intergrown with altered amphibole. The groundmass consists of amorphous clays, some poorly defined feldspars (altered to clays), magnetite, locally minor recrystallized spherulites, and chloritoid, and few partly deformed phenocrysts of biotite. Zircon, hematite/goethite and apatite occur as accessory phases in these biotite-rich porphyritic quartz andesites.

3.1.2. Hornblende-rich porphyritic andesite (Karakise Tepe andesite)

This adakitic rock in the Kale area is well-exposed around Karakise Hill and occupies ca. 0.5 km² at the northwestern part of the study area (Figs. 3 and 4C). In this location, the intrusive cuts sedimentary rocks of late Cretaceous Kermutdere Formation and is covered by nummulite-bearing limestones. The rock is generally massive and well jointed, and characterized by abundant slender amphibole crystals visible in the hand specimen. It is whitish gray to dark gray depending on the ratio of amphibole phenocrysts and the degree of alteration of the plagioclases. In thin section, the rock is porphyritic hornblende andesite. Medium-grained oxy-hornblende occurs as subhedral/euhedral phenocrysts, whereas the phenocrysts of plagioclase are altered and partly recrystallized. The groundmass consists predominantly of small, sub to anhedral laths of plagioclase and interstitial, poorly defined K-feldspars. Fine-grained magnetite is disseminated through the groundmass, and also occurs as a minor replacement product after hornblende. The rock is extensively oxidized and the hornblende phenocrysts are rimmed by a dark oxidized rim. Most amphibole phenocrysts are zoned, and some are completely altered to amorphous Fe-hydroxide. The feldspars are partly recrystallized, and contain minute inclusions of Fe-hydroxide. Fine-grained carbonate represents minor alteration in the rock, occurring interstitial and partly

replacing some of the plagioclase. Zircon and apatite occur as accessory phases in the rock.

3.1.3. Andesitic hyaloclastite breccia

This unit is well-exposed at the base of the early Cenozoic Alibaba Formation and reaches a thickness of 50 m in some places (Figs. 3 and 4C–F). Angular and hornblende-rich andesite clasts occur within a fine-grained, dark red colored, sedimentary and fossiliferous matrix (Fig. 4E). The size of andesite clasts varies from a few mm to 50 cm. In thin section, the clasts consist predominantly of zoned plagioclase phenocrysts and glomerocrysts, zoned and unzoned hornblende phenocrysts and glomerocrysts, and fine-grained groundmass consisting of mottled, clay-altered and clear, unaltered feldspars, lesser, fine-grained amphibole and magnetite. Relatively coarse-grained and zoned subhedral/euhedral plagioclase occurs as phenocrysts. Most grains show a mottled reaction rim, suggesting compositional variation between the core and rim. Single twinning is common, but much of the polysynthetic twinning has been destroyed. The groundmass feldspars show single twinning and are mostly tablet-shaped, zoned equant grains. Fine- to medium-grained hornblende occurs as subhedral/euhedral phenocrysts, as relatively fine-grained aggregates and as small grains within the groundmass. They are pleochroic, variably zoned grains, and most are rimmed by mottled, microcrystalline Fe-hydroxide. The dark center and lighter rim in some of the phenocrysts suggest compositional zoning. The clear, equant, tablet-shaped feldspars in the matrix possess single twinning and some feldspars are lath-shaped. They are too fine-grained for optical identification. The shape and single twinning would be consistent with K-feldspar, although the zoning suggests plagioclase. Fine-grained magnetite is disseminated throughout the groundmass.

3.1.4. Kircaova dacite

This body occupies about 0.8 km² at the southeastern part of the map area (Fig. 3) and is easily distinguished from other adakitic bodies by its yellowish gray and beige colors in the field, and by the quartz phenocrysts in the hand specimen. In thin section, the rock is a porphyritic dacite and consists of coarse to relatively fine-grained phenocrysts of plagioclase, quartz and lesser, small phenocrysts of amphibole. The groundmass consists of fine-grained subhedral plagioclase, K-feldspars, anhedral carbonate and minor quartz. Plagioclase occurs as single grains and also in aggregates forming clusters (glomerocrysts) with or without quartz. All of the large phenocrysts are cloudy and turbid, with the exception of the center of some grains. The composition – where it was possible to determine, is An_{15–25}. A few of the large, turbid phenocrysts have relict zoning. The quartz phenocrysts have resorbed and embayed grain boundaries, and some phenocrysts occur in aggregates with the plagioclase, forming glomerocrysts. Euhedral to subhedral small prisms of amphibole phenocrysts are weakly pleochroic green, and most are partly replaced by carbonate, and rimmed by amorphous, dark Fe-rich clays. The long, prismatic phenocrysts are fractured and some are fragmented. Fine-grained, anhedral magnetite is relatively abundant in the groundmass, and some are partly replaced by hematite.

3.2. Non-adakitic magmatism

This volcanic sequence known as Alibaba Formation is well-exposed in the Gumushane area and its vicinity. Similar volcanic rocks in composition and age also appear along an approximately E–W trending zone in the southern part of the eastern Pontides orogenic belt. In the study area (Kale–Gumushane), the main lithologies include hornblende-rich volcanic rocks, basaltic-andesitic pyroclastic rocks, and also basic volcanic rocks representing the final stage of the basic volcanism in the region

occurring as dikes that cut across the other lithologies of the Alibaba Formation (Fig. 3).

3.2.1. Hornblende-rich andesite (*Pirahmet andesite*)

The coarse-grained hornblende-rich volcanic rocks are widely exposed as small ellipsoidal intrusions and/or rarely as dikes cutting the late Cretaceous Kermutdere Formation, late Jurassic–early Cretaceous Berdiga Formation, the late Carboniferous Gumushane granitoid and the basement units of the early Cenozoic Alibaba Formation (Fig. 3). The main outcrops occur at the northwestern part of the map area (Fig. 3). These non-adakitic volcanic rocks in the Kale (Gumushane) area are characterized by abundant euhedral to subhedral hornblende phenocrysts in a greenish gray and fine-grained groundmass in hand specimen. In thin section, the rock is a coarse-grained porphyritic hornblende andesite. The rock consists mainly of zoned and partly recrystallized phenocrysts of plagioclase, euhedral to subhedral phenocrysts and glomerocrysts of hornblende, small phenocrysts of biotite, and a relatively abundant magnetite and ilmenite. Anhedral to subhedral plagioclase phenocrysts make up a significant part of the rock and are partly to completely recrystallized to fine-grained aggregates. Some of these are partly replaced by quartz. The hornblende phenocrysts are unzoned, and most are relatively unaltered. Most hornblende crystals are rimmed by amorphous Fe-hydroxide. There is textural evidence to suggest the original presence of biotite, although these have recrystallized to very fine-grained aggregates. The fine-grained groundmass is mottled, variably anisotropic, and consists mostly of clay-altered feldspars, and some of the plagioclases are rimmed by fine-grained, Fe-stained secondary biotite.

3.2.2. Basaltic-andesitic pyroclastic rocks

In the Kale area, the pyroclastic members of the early Cenozoic Alibaba Formation are mainly represented by agglomerate, and minor volcanic breccia tuff and tuffite. The agglomerates are the volumetrically dominant lithology in the pyroclastic sequence. They consist of rounded bombs, which are generally larger than 5 cm in diameter, within a medium-grained, strongly altered and grayish-brownish subordinate groundmass. Exfoliation structure and calcite-filled fractures are common. They are generally hornblende-poor. However, hornblende-rich lithologies can be seen at the upper part of the sequence. In thin section, the hornblende-poor bombs consist predominantly of plagioclase and minor clinopyroxene. Plagioclase occurs as large, lath-shaped phenocrysts and as small microlite interstitial to the groundmass. The phenocrysts are pervasively altered and partly recrystallized. Replacement minerals include sericite, carbonate, chlorite and minor epidote. The clinopyroxene occurs as unzoned, subhedral grains interstitial to the plagioclase. Some are partly altered at the grain boundaries to clays. Anhedral grains of magnetite are disseminated through the rock. In the hornblende-rich clasts, the rock consists predominantly of partly or completely-altered plagioclase and slender hornblende. Much of the rock is made up of lath-shaped and needle-shaped plagioclase. The composition cannot be determined, as the twin lamellae were partly destroyed. Fine- to medium-grained hornblende occurs as subhedral/euhedral phenocrysts. They are pleochroic, and most are rimmed by Fe-hydroxide. Fine-grained magnetite is randomly distributed through the groundmass. Zircon and apatite occur as accessory phases in both rock types. The tuffs interbedded with the tuffites are gray to greenish gray in color. On the weathered surfaces, the rock is characteristically yellowish to whitish gray. In thin section, they are andesitic crystal tuff. The tuffites are characterized by the presence of large nummulites reaching 3 cm in length. Layering is well developed in agglomerates and other pyroclastic members of the Alibaba Formation and the layers vary from less than 1 m to several meters in thickness.

3.2.3. Basic dikes

The basic dikes up to 3 m wide intrude the pyroclastic members of the Alibaba Formation (Figs. 3 and 4C). They are the youngest intrusions in the study area and are of late Eocene or younger in age. Their dominant orientation is northeast-southwest with near-vertical dips. The rock is characterized by abundant plagioclase phenocrysts within a fine- to medium-grained groundmass in hand specimen. The fresh surfaces are medium to dark gray in color. On the weathered surfaces, it is characteristically brownish to whitish gray depending on the degree of alteration of plagioclase phenocrysts. In thin section, the subhedral to euhedral plagioclase makes up a significant part of the rock and occurs as phenocrysts and as glomerocrysts. Some plagioclases are zoned and some have polysynthetic twinning. They are relatively unaltered, with the exception of minor sericite and cross-cutting veinlets that consist of clays. The composition of plagioclase ranges between oligoclase and andesine. The groundmass plagioclase is mostly tablet-shaped and equant grains. Single twinning is common. Fine-grained, unzoned, weakly pleochroic green and anhedral augite is generally interstitial to the plagioclase phenocrysts. The groundmass consists of plagioclase, augite, and opaque grains.

4. Whole rock geochemistry

In order to interpret the origin and geodynamic setting of the Cenozoic magmatic rocks in the investigated area, major-trace and rare earth element contents of 76 samples were analyzed at the ACME Analytical Laboratories in Canada. The major oxides and Sc were determined using ICP-ES method and trace and rare earth elements were analyzed by ICP-MS method. The sample digestion procedures are similar for both ICP-MS and ICP-ES. 0.2 g of pulverized sample is weighed into a graphite crucible and mixed with 1.5 g of LiBO₂ flux. The mixture is heated in a muffle furnace for 15 min at 1050 °C. The molten mixture is removed and quickly poured into 100 mL of 5% HNO₃. This solution is shaken for 2 h and the aliquot is transferred into a polypropylene test tube. Standards and reagent blanks are added to the sample sequence. At the second stage (sample analysis), sample solutions are aspirated into an ICP mass spectrometer (Perkin-Elmer Elan 6000) or an ICP emission spectrometer (Jarrel Ash Atomcomp Model 975) for determination of element content. The results are presented in Tables 1–4.

Biotite-rich andesites (Kizil Tepe andesite) are characterized by 58.81–62.71 wt.% SiO₂, 15.01–16.96 wt.% Al₂O₃, 2.82–4.64 wt.% Na₂O, 3.58–4.38 wt.% FeO^t, 0.35–0.47 wt.% TiO₂, 1.72–3.29 wt.% MgO, 4.08–5.86 wt.% CaO, 1.33–2.73 wt.% K₂O, 475–787 ppm Sr, 9.5–11.8 ppm Y, 15.7–77.3 ppm Ni, 30.1–70.8 ppm Rb, 84.2–160.5 ppm Zr, 15.7–24.9 ppm La and 0.86–1.11 ppm Yb (Table 1). Their Mg numbers are between 47.2 and 61.7. When compared with the biotite-rich andesites, the hornblende-rich andesites (Karakise Tepe andesite) are characterized by relatively high TiO₂ (0.42–0.55 wt.%), Na₂O (4.05–6.03 wt.%), K₂O (1.5–3.82 wt.%), Sr (809–1207 ppm), low MgO (0.82–1.39 wt.%), Y (4.8–6.4 ppm), Yb (0.43–0.50 ppm), Ni (3.2–6.4 ppm) contents and Mg numbers between 31.2 and 42.2 (Table 2). The hornblende-rich andesitic clasts taken from hyaloclastite breccia horizon occupying the basement of the Alibaba Formation in the Yeniyol and Kale areas contain 59.72–65.72 wt.% SiO₂, 0.36–0.44 wt.% TiO₂, 15.35–17.65 wt.% Al₂O₃, 3.54–4.39 wt.% FeO^t, 1.38–2.27 wt.% MgO, 2.94–5.04 wt.% CaO, 3.58–5.9 wt.% Na₂O, 1.62–3.11 wt.% K₂O, 6.6–18.8 ppm Ni, 433–778 ppm Sr, 9.6–12.6 ppm Y, 26.9–70.1 ppm Rb, 76–93 ppm Zr, 9.7–13.3 ppm La and 0.85–1.06 ppm Yb (Table 2). The dacitic rocks (Kircaova dacite) are geochemically distinguished from the other three groups mentioned above with their relatively high-SiO₂ (66.57–69.02 wt.%), Na₂O (4.8–6.78 wt.%), and low MgO (0.26–0.47 wt.%), FeO^t (2.5–3.16 wt.%), CaO

Table 1

Major, trace and rare earth element concentrations of biotite-rich adakitic andesites (Kizil Tepe andesite) from the Kale area.

Sample	HT-1	HT-2	HT-3	HT-4	AR-1	AR-2	AR-3	AR-4	AR-6	HT-40	HT-42	HT-43	HT-44	HK-1	HK-2	HK-3	HK-4
Rock type	Biotite-rich adakitic andesite (Kizil Tepe andesite)																
Location	Harmancık Hill				Kizil Hill				Unnamed Hill (north of Guney Hill)					Yikintibasi Hill			
SiO ₂	60.12	60.62	60.05	60.41	59.87	62.34	60.89	59.5	60.75	60.64	61.95	62.56	62.71	61.74	58.81	60.2	60.48
TiO ₂	0.42	0.46	0.47	0.46	0.36	0.36	0.36	0.38	0.37	0.37	0.38	0.39	0.38	0.36	0.35	0.35	0.35
Al ₂ O ₃	15.38	15.36	15.01	15.03	16.03	16.01	16.65	16.4	16.83	15.93	16.06	16.96	16.74	16.64	15.91	16.06	16.37
Fe ₂ O ₃	4.21	4	3.93	4.03	3.97	3.84	3.87	4.05	3.94	4.06	4.08	4.12	4.38	3.74	3.88	3.79	3.58
MnO	0.07	0.06	0.06	0.06	0.09	0.08	0.08	0.1	0.08	0.08	0.06	0.05	0.04	0.03	0.04	0.03	0.03
MgO	2.72	2.5	2.85	2.62	3.08	3	3.11	3.29	3.16	2.13	2.21	2.23	2.18	1.86	1.75	1.72	1.96
CaO	5.02	4.97	5.32	5.12	5.21	4.99	4.83	5.11	4.78	6.11	5.14	4.4	4.08	4.98	6.58	5.86	5.48
Na ₂ O	3.44	3.38	3.33	3.31	4.23	3.88	4.4	4.44	4.51	3.98	4.48	4.39	4.64	3.71	2.94	2.82	3.23
K ₂ O	2.65	2.73	2.7	2.7	1.33	1.69	1.64	1.42	1.69	1.82	1.88	1.91	1.9	1.6	1.89	2	1.81
P ₂ O ₅	0.32	0.26	0.27	0.26	0.17	0.15	0.18	0.17	0.16	0.17	0.17	0.18	0.18	0.16	0.145	0.138	0.157
Cr ₂ O ₃	0.015	0.016	0.016	0.016	0.007	0.008	0.007	0.01	0.008	0.004	0.004	0.004	0.004	<0.002	<0.002	0.004	0.003
LOI	5.6	5.4	5.7	5.7	5.4	3.4	3.7	4.9	3.5	4.5	3.4	2.5	2.5	5.1	6.5	6.8	6.5
Total	99.97	99.76	99.71	99.72	99.75	99.75	99.72	99.77	99.78	99.79	99.81	99.69	99.73	99.92	98.80	99.77	99.95
Mg [#]	56.1	55.3	59.0	56.3	60.6	60.7	61.4	61.7	61.4	51.0	51.8	51.7	49.6	49.6	47.2	47.3	52.0
Na ₂ O + K ₂ O	6.09	6.11	6.03	6.01	5.56	5.57	6.04	5.86	6.2	5.8	6.36	6.3	6.54	5.31	4.83	4.82	5.04
Sc	8	9	9	9	10	10	9	9	9	9	9	10	9	9	8	8	8
V	69	72	70	73	77	80	76	80	79	77	82	90	86	72	71	70	69
Co	12.2	11.8	12.4	12.4	10.8	11.5	10.6	10.8	11.3	11.4	10.8	11.9	10.9	8.4	10.7	10.5	8.9
Ni	68.4	72.8	74.3	77.3	14.9	15.9	15.7	16	16.9	24.4	26.8	32.2	30.6	32.4	34.7	34.3	31.8
Cr	102.8	109.7	109.7	109.7	48.0	54.8	48.0	54.8	54.8	27.4	27.4	27.4	27.4	—	—	27.4	20.6
Cu	8.4	8.6	8.8	9.3	23	14.2	12.8	13.9	11.8	14.8	13.6	11.3	13.3	12	12.9	14.9	13.3
Zn	48	53	44	47	44	41	46	47	47	49	47	46	47	42	43	40	48
Ga	15.3	15.4	15.6	15.1	15.8	17.5	18	15.7	16.5	16.2	16.8	17.1	17.1	16.8	16.5	17.2	17.9
Cs	0.6	0.6	0.6	0.6	0.2	0.1	0.2	0.1	0.1	0.6	0.5	0.4	0.4	0.5	0.7	0.5	0.5
Rb	69.4	70.8	68.3	67.6	28.3	36.2	33.4	30.1	33.8	36.2	37.8	38.3	38.1	30.2	36.2	38.3	32.9
Ba	740	727	726	728	481	604	585	508	601	628	678	689	652	617	455	484	478
Sr	642.7	612.7	633.5	609.9	679.7	734.5	752.6	684	710.9	719.9	766.8	786.5	758.4	552.5	555.1	477.5	475.5
Y	10.6	10.4	9.2	10.4	10.3	10.1	10.1	11	10.6	11.1	10.7	10.5	11.8	10.1	10.4	10.4	9.5
Zr	159.4	160.5	165	157.2	90.6	92.1	90.5	86.7	84.2	89.3	92.6	94.6	94.4	87.8	86.3	88.2	86.7
Nb	11.6	11.3	11.7	11.2	6.2	6.5	6.4	7.3	7	6.2	6.4	6.6	6.8	6.6	6.5	6.8	7
Hf	4.3	4.6	4.9	4.8	2.6	2.5	2.4	2.4	2.5	2.3	2.5	2.7	2.9	2.5	2.4	2.4	2.6
Ta	0.6	0.6	0.6	0.6	0.4	0.4	0.3	0.3	0.1	0.3	0.3	0.4	0.4	0.4	0.4	0.4	0.4
Pb	7.6	8	3.7	3.8	8.1	6.1	6.4	9	6.2	3.1	3.6	3.4	3.9	2.2	1.8	2.1	2.3
Th	3.6	3.4	3.8	3.6	4.3	4.8	4.4	3.9	4.4	4.5	4.6	4.7	5	2.4	2.8	2.3	2.5
U	1.2	1.2	1.2	1.2	1.2	1.2	1.2	1.1	1.1	1.1	1.1	1.1	1.2	0.9	0.8	0.9	1
La	19.2	19.8	19.8	19.5	17.7	17.7	18.3	19.6	19.9	22.8	23.2	24.5	24.9	16.6	16.8	16.3	15.7
Ce	38.7	39.1	40.2	38.6	38	38.8	38.4	37.8	40.3	42.7	43.5	45.8	44.8	31.5	32.7	31.1	31
Pr	4.36	4.52	4.53	4.41	4.03	4.23	4.03	4.17	4.35	4.76	4.94	5.33	5.22	3.7	3.79	3.59	3.54
Nd	16.6	16.8	17.8	16.4	15.2	16.1	15	16.5	17	18.4	19.2	20.4	20	13.9	13.9	14.4	13.3
Sm	2.66	2.72	2.72	2.75	2.77	2.77	2.73	2.77	2.79	2.88	2.98	3.25	3.19	2.48	3	2.5	2.38
Eu	0.75	0.82	0.8	0.79	0.79	0.79	0.8	0.87	0.8	0.85	0.91	0.93	0.97	0.76	0.79	0.78	0.75
Gd	2.08	2.14	2.06	2.17	2.22	2.34	2.21	2.34	2.26	2.32	2.36	2.4	2.57	2.21	2.22	2.24	2
Tb	0.34	0.33	0.3	0.31	0.35	0.35	0.34	0.36	0.33	0.34	0.35	0.36	0.38	0.33	0.35	0.33	0.31
Dy	1.68	1.71	1.6	1.71	1.69	1.76	1.92	1.93	1.8	1.77	1.86	1.92	1.98	1.71	1.71	1.57	1.68
Ho	0.32	0.34	0.31	0.33	0.36	0.36	0.35	0.37	0.36	0.33	0.36	0.35	0.38	0.35	0.34	0.36	0.32
Er	0.88	0.96	0.86	0.91	1.02	1.03	0.98	1.08	0.99	0.98	0.97	0.95	1.1	0.93	0.98	0.97	0.84
Tm	0.14	0.15	0.13	0.15	0.16	0.15	0.16	0.17	0.15	0.15	0.16	0.16	0.16	0.15	0.14	0.16	0.14
Yb	0.96	0.97	0.91	1	0.95	1.11	1.08	1.17	1.06	1	1	0.99	1.12	0.99	0.99	1.03	0.86
Lu	0.16	0.15	0.13	0.16	0.17	0.16	0.17	0.18	0.16	0.15	0.15	0.15	0.17	0.15	0.16	0.17	0.15
Sr/Y	60.6	58.9	68.9	58.6	66.0	72.7	74.5	62.2	67.1	64.9	71.7	74.9	64.3	54.7	53.4	45.9	50.1
(La/Yb) _N	20.0	20.4	21.8	19.5	18.6	15.9	16.9	16.8	18.8	22.8	23.2	24.7	22.2	16.8	17.0	15.8	18.3

Table 2

Major, trace and rare earth element concentrations of hornblende-rich adakitic andesites (Karakise Tepe andesite) and andesitic hyaloclastite breccia from the Kale area.

Sample	HT-132	HT-133	HT-136	HT-137	HT-138	AR-16	AR-24	AR-13	AR-29	HT-37	HT-118	HT-125	HT-126	HT-127	HT-128	HT-111	HT-113
Rock type	Hornblende-rich adakitic andesite (Karakise Tepe andesite)										Andesite hyaloclastite breccia						
Location	Karakise Hill					Pirlikiran Hill					Yeniyol			Kale			
SiO ₂	61.18	61.29	62.28	63.07	62.44	62.9	63.07	61.6	64.76	64.12	65.54	59.72	60.34	62.58	61.44	64.94	65.72
TiO ₂	0.5	0.49	0.48	0.52	0.42	0.5	0.47	0.55	0.43	0.45	0.38	0.41	0.42	0.40	0.44	0.39	0.36
Al ₂ O ₃	16.65	16.01	16.34	16.45	16.13	16.28	17.22	17.55	17.94	17.26	16.59	17.65	17.65	17.14	16.98	16.68	15.35
Fe ₂ O ₃	3.58	3.36	3.12	3.26	3.44	3.71	3.51	3.96	3.02	3.84	3.54	4.39	4.08	4.22	3.86	3.89	3.79
MnO	0.03	0.03	0.04	0.03	0.03	0.04	0.04	0.04	0.03	0.04	0.05	0.13	0.14	0.15	0.15	0.04	0.05
MgO	1.28	1.22	1.14	1.18	1.27	1.14	1.31	1.39	0.82	0.88	1.77	2.12	2.27	2.02	1.98	1.38	1.76
CaO	4.38	5.53	4.78	5.22	4.84	5.83	3.82	2.16	3.94	4.18	5.04	3.36	3.34	3.42	4.02	2.94	4.65
Na ₂ O	4.81	4.05	5.02	4.84	4.93	5.85	5.48	6.03	5.26	5.66	3.8	5.9	5.83	4.84	5.44	5.77	3.58
K ₂ O	2.41	1.97	2.14	2.18	1.94	1.5	2.61	3.82	1.85	1.87	1.9	3.08	3.11	2.98	3.12	1.62	2.55
P ₂ O ₅	0.23	0.23	0.21	0.22	0.2	0.24	0.22	0.27	0.2	0.21	0.14	0.14	0.15	0.14	0.14	0.18	0.16
Cr ₂ O ₃	<0.002	0.003	0.002	0.003	0.003	0.002	0.002	<0.002	<0.002	<0.002	0.007	0.008	0.006	0.007	0.008	0.007	0.006
LOI	4.7	5.6	4.3	2.9	4.1	1.8	2	2.2	1.5	1.3	1	2.8	2.4	1.9	2.2	1.9	1.8
Total	99.75	99.78	99.85	99.87	99.74	99.79	99.75	99.57	99.75	99.81	99.76	99.71	99.74	99.80	99.78	99.74	99.78
Mg [#]	41.5	41.8	42.0	41.8	42.2	37.8	42.5	41.0	35.0	31.2	49.8	48.9	52.4	48.7	50.4	41.3	47.9
Na ₂ O + K ₂ O	7.22	6.02	7.16	7.02	6.87	7.35	8.09	9.85	7.11	7.53	5.7	8.98	8.94	7.82	8.56	7.39	6.13
Sc	7	7	6	7	6	6	6	8	5	5	11	11	12	11	12	8	10
V	81	80	78	82	80	91	72	85	68	67	82	91	105	87	94	69	88
Co	7.8	7.2	6.8	7.3	7.1	8.4	7.2	7.7	5.6	5.6	8.3	13	13.5	12.8	11.4	6.5	8.1
Ni	6.3	3.3	5.4	5.1	4.8	5.7	6.4	6.3	3.2	3.6	7.4	15.8	7.9	11.6	12.7	18.8	6.6
Cr		20.6	13.7	20.6	20.6	13.7	13.7		48.0	54.8	41.1	48.0	54.8	48.0	54.8	48.0	41.1
Cu	6.7	5.2	6.8	7.4	6.5	13.8	5.6	24.3	4.5	8.1	21.2	7.3	5.2	14.1	8.5	6.8	23.2
Zn	45	43	41	38	40	38	41	52	28	38	25	35	36	27	32	42	30
Ga	19.1	19.1	18.6	19.4	18.8	14	17.3	15.9	13.4	14.8	14.8	15	15.2	15.2	15	13.8	13.3
Cs	0.4	0.4	0.3	0.4	0.4	0.3	0.6	0.8	0.7	0.3	0.3	0.6	0.5	0.6	0.4	0.3	0.3
Rb	40.2	33.9	35.7	36.42	38.5	13.3	36.7	69.6	28.5	16	41.3	70.1	64.6	48.6	65.7	26.9	46
Ba	706	546	628	579	604	221	586	1633	541	302	1042	847	913	947	996	662	738
Sr	1206.2	1047.9	1128	986.7	1144.6	809.3	1071.9	1746.4	1092	848.1	433.3	744.4	777.3	686.2	721.1	699.7	443.6
Y	4.9	5.2	5.3	4.8	5.6	6.3	5.8	6.4	5.2	5.6	11.2	9.6	10.1	10.2	10.7	9.6	12.6
Zr	94.1	92.9	96.8	100.2	97.4	91.7	100.5	96.7	92.6	91.6	78.8	86.7	93	82.4	85.8	89.3	76.5
Nb	5	4.9	4.8	4.9	4.8	5.2	5.5	5.4	5.1	5.2	5.2	5.6	6	5.4	5.6	6.2	5.1
Hf	2.6	2.9	2.7	2.9	2.7	2.5	2.9	2.8	2.5	2.7	2.2	2.7	2.4	2.3	2.3	2.5	2
Ta	0.2	0.2	0.3	0.2	0.2	0.2	0.3	0.2	0.2	0.3	0.3	0.4	0.3	0.3	0.3	0.4	0.3
Pb	7.5	7.1	6.7	7.4	7.7	3	4.4	8.1	2.6	4.7	5.6	3.3	4.1	4.8	3.9	5.5	4.9
Th	2.9	3.1	2.9	3.1	3.2	3.2	3.8	3.2	3.4	3.3	3.1	3.3	3.1	3.1	3.2	2.1	3.1
U	0.6	0.6	0.7	0.7	0.6	0.8	0.8	0.8	0.7	0.8	0.8	0.7	0.7	0.8	0.7	0.5	0.6
La	19.6	19.5	18.7	19.6	20.1	20.5	20.4	22.3	15.9	20.7	13.3	9.7	11.4	11.8	12.4	14.3	14.1
Ce	43.2	42	41.2	42.4	43.6	42.9	44.8	43.8	35.2	42.2	27.5	24.1	27.6	25.2	26.3	29.9	28.1
Pr	4.55	4.52	4.34	4.25	4.12	4.84	4.88	5.24	3.95	4.68	3.02	2.89	3.2	3.42	3.73	3.65	3.22
Nd	16.8	17.2	16.2	16.6	17.1	18	18.4	20.1	14.8	17.1	12.3	11.5	13	11.8	12.6	14.6	13
Sm	2.58	2.53	2.51	2.56	2.48	2.74	2.71	3.06	2.13	2.43	2.35	2.35	2.52	2.44	2.38	2.64	2.4
Eu	0.79	0.73	0.73	0.78	0.81	0.81	0.8	0.91	0.64	0.76	0.72	0.69	0.83	0.77	0.74	0.77	0.76
Gd	1.76	1.7	1.68	1.74	1.74	1.87	1.69	1.99	1.5	1.65	2.12	2.06	2.22	2.04	2.12	2.16	2.28
Tb	0.23	0.22	0.24	0.26	0.25	0.25	0.23	0.27	0.2	0.22	0.33	0.33	0.34	0.37	0.34	0.34	0.35
Dy	1.12	1.02	1.06	0.98	1.16	1.17	1.1	1.26	0.88	1	1.81	1.67	1.81	1.76	1.74	1.7	1.93
Ho	0.17	0.18	0.16	0.18	0.18	0.21	0.2	0.21	0.17	0.18	0.36	0.33	0.34	0.38	0.32	0.33	0.41
Er	0.48	0.49	0.42	0.47	0.51	0.57	0.55	0.56	0.49	0.47	1.07	0.89	0.98	0.94	1.02	0.9	1.07
Tm	0.07	0.07	0.08	0.06	0.07	0.09	0.08	0.08	0.07	0.07	0.15	0.13	0.15	0.16	0.15	0.13	0.17
Yb	0.45	0.4	0.47	0.45	0.47	0.48	0.5	0.5	0.46	0.43	1.01	0.89	0.95	0.92	0.85	0.88	1.06
Lu	0.06	0.06	0.06	0.06	0.07	0.08	0.08	0.08	0.07	0.06	0.15	0.12	0.13	0.17	0.14	0.12	0.16
Sr/Y	246.2	201.5	212.9	205.6	204.4	128.5	184.8	272.9	209.9	151.4	38.7	77.5	77.0	67.3	67.4	72.9	35.2
(La/Yb) _N	43.6	48.8	39.8	43.6	42.8	42.7	40.8	44.6	34.6	48.1	13.2	10.9	12.0	12.8	14.6	16.3	13.3

Table 3
Major, trace and rare earth element concentrations of adakitic dacites (Kircaova dacite) and non-adakitic hornblende-rich andesites (Pirahmet andesite) from the Kale area.

Sample	HT-56	HT-57	HT-58	HT-59	HT-60	HT-61	HT-62	HT-63	AR-47	AR-49	AR-50	AR-51	AR-53	AR-55
Rock type	Adakitic dacite (Kircaova dacite)								Non-adakitic hornblende-rich andesite (Pirahmet andesite)					
Location	Kircaova								Pirahmet					
SiO ₂	66.72	68.75	69.02	66.57	68.82	67.86	67.49	68.12	56.42	56.16	56.4	56.32	54.74	56.03
TiO ₂	0.41	0.35	0.37	0.36	0.42	0.38	0.37	0.44	0.58	0.58	0.59	0.58	0.64	0.55
Al ₂ O ₃	17.39	15.53	15.22	16.63	15.98	16.48	17.02	16.64	17.66	17.65	17.71	17.76	17.94	17.58
Fe ₂ O ₃	2.5	2.69	2.8	3.14	2.9	2.88	3.02	3.16	7	6.99	7.01	7.27	7.75	6.97
MnO	0.03	0.03	0.03	0.02	0.02	0.03	0.03	0.02	0.15	0.15	0.17	0.14	0.17	0.15
MgO	0.26	0.39	0.38	0.47	0.36	0.42	0.36	0.32	2.99	3.02	3.27	3.03	3.65	2.92
CaO	2.16	3.08	3.12	3.32	3.02	2.86	3.14	2.96	5.91	5.93	5.16	5.34	6.31	6.21
Na ₂ O	6.78	5.29	5.28	4.8	4.89	5.34	5.02	4.96	4.06	4	4.36	4.31	3.42	3.77
K ₂ O	1.8	1.31	1.61	1.75	1.74	1.78	1.92	1.65	1.27	1.24	1.5	1.64	0.83	1.25
P ₂ O ₅	0.19	0.17	0.18	0.16	0.19	0.16	0.18	0.17	0.25	0.26	0.26	0.26	0.16	0.19
Cr ₂ O ₃	0.007	0.006	0.006	0.007	0.007	0.006	0.006	0.008	<0.002	<0.002	<0.002	<0.002	<0.002	<0.002
LOI	1.6	2.2	1.9	2.6	1.6	1.7	1.4	1.5	3.5	3.8	3.3	3.1	4.2	4.2
Total	99.85	99.80	99.92	99.83	99.95	99.90	99.96	99.95	99.79	99.78	99.73	99.75	99.81	99.82
Mg [#]	17.1	22.3	21.2	22.9	19.7	22.4	19.1	16.7	45.8	46.1	48.0	45.2	45.2	45.4
Na ₂ O + K ₂ O	8.58	6.6	6.89	6.55	6.63	7.12	6.94	6.61	5.33	5.24	5.86	5.95	4.25	5.02
Sc	6	6	6	5	5	5	5	6	12	12	13	12	20	15
V	60	50	55	55	60	64	66	58	119	117	118	111	185	128
Co	3.1	5.9	4.8	5.9	5.3	4.2	5.1	5.2	12.4	12.8	12.6	12.3	20	14.4
Ni	22.7	26.4	25.2	30.3	26.1	24.8	25.2	25.6	4.3	1.9	2	2.4	3.5	1.9
Cr	48.0	41.1	41.1	48.0	48.0	41.1	41.1	54.8						
Cu	16	16.3	16.7	18.7	16.9	17.4	16.2	15.8	14.1	14.3	14.9	12.3	39.1	16.4
Zn	38	49	52	51	54	56	54	47	46	41	60	45	51	54
Ga	10.7	12.3	11.4	13.4	12.1	11.6	10.8	11.2	15.8	16.2	16.1	16.5	15	14.6
Cs	0.3	0.2	0.2	0.2	0.2	0.3	0.2	0.2	0.4	0.4	0.3	0.3	0.3	0.4
Rb	19.5	14.5	16.5	16.3	17.6	18.2	16.7	19.1	28.9	28.4	36.4	41.3	21.3	24.4
Ba	466	423	488	528	473	494	502	482	425	442	503	495	250	500
Sr	758.7	652.8	704.3	610.1	716.6	726.9	688.5	702.7	439.3	442.9	445.3	445	421.8	472.6
Y	8.6	7.8	7.9	7.1	8.2	9.1	8.4	7.6	19.4	19.8	19.7	19.3	19.8	17.6
Zr	85.1	80.2	82.2	81.1	84.1	86.8	91.2	85.4	123.9	122.1	118.5	120.5	72	100.7
Nb	6.6	6.1	6.4	6.3	6.2	5.9	6.1	6.3	6.9	7.1	6.6	6.7	4	5.8
Hf	2.2	2.4	2.1	2.4	2.3	2.2	2.1	2.4	3.1	3.1	3.4	3	2.2	2.8
Ta	0.3	0.3	0.3	0.3	0.3	0.2	0.2	0.3	0.3	0.3	0.3	0.4	0.2	0.3
Pb	3.6	3.9	3.7	4	3.9	3.9	3.4	4.1	2.2	2.3	2.4	1.9	1.6	4
Th	2.2	2.3	2.4	2.3	2.6	2.5	2.4	2.6	2.7	2.9	2.5	2.6	2	2.4
U	0.8	0.7	0.7	0.7	0.7	0.5	0.6	0.8	0.5	0.5	0.5	0.5	0.4	0.5
La	14.8	15.5	15.6	14.8	15.2	14.7	15.2	14.6	18.3	18.4	18.3	18.1	12.6	16.2
Ce	30.1	31.5	30.6	30	31.2	33.2	31.4	32.1	39.7	40.4	39.7	39.6	28	34
Pr	3.57	3.55	3.48	3.44	3.44	3.41	3.36	3.62	4.99	4.96	4.91	4.96	3.62	4.08
Nd	14.1	14.4	14.6	13.1	14.2	13.8	14.7	14.2	20.2	20.6	20.2	18.9	15.2	16.3
Sm	2.39	2.3	2.41	2.23	2.38	2.26	2.38	2.43	3.87	3.9	3.92	3.91	3.28	3.36
Eu	0.71	0.68	0.67	0.68	0.67	0.7	0.64	0.66	1.18	1.17	1.17	1.17	1.03	1.01
Gd	1.95	1.8	1.85	1.67	1.92	1.78	1.66	1.84	3.68	3.63	3.6	3.7	3.42	3.1
Tb	0.28	0.26	0.27	0.25	0.26	0.25	0.25	0.28	0.58	0.59	0.57	0.58	0.57	0.51
Dy	1.42	1.35	1.42	1.28	1.44	1.46	1.32	1.36	3.37	3.36	3.28	3.32	3.38	2.93
Ho	0.28	0.25	0.26	0.24	0.24	0.26	0.27	0.31	0.65	0.66	0.66	0.65	0.68	0.6
Er	0.78	0.71	0.76	0.65	0.72	0.68	0.75	0.75	1.99	1.87	1.92	2.07	2.07	1.76
Tm	0.12	0.1	0.11	0.09	0.12	0.09	0.1	0.11	0.32	0.32	0.32	0.32	0.34	0.29
Yb	0.71	0.66	0.68	0.59	0.66	0.64	0.72	0.68	1.99	2.04	1.99	1.94	2.08	1.81
Lu	0.11	0.1	0.12	0.09	0.14	0.13	0.11	0.11	0.32	0.33	0.32	0.32	0.32	0.28
Sr/Y	88.2	83.7	89.2	85.9	87.4	79.9	82.0	92.5	22.6	22.4	22.6	23.1	21.3	26.9
(La/Yb) _N	20.8	23.5	22.9	25.1	23.0	23.0	21.1	21.5	6.2	6.1	6.2	6.3	4.1	6.0

(2.16–3.32 wt.%) and Rb (14.5–19.5 ppm) contents (Table 3). They also include high concentrations of Al₂O₃ (15.22–17.39 wt.%) and Sr (610–759 ppm), and low concentrations of TiO₂ (0.35–0.42 wt.%), Y (7.1–9.1 ppm) and Yb (0.59–0.72 ppm). It is clear that all of these four groups reveal the geochemical features of adakitic rocks, which was first named by Defant and Drummond (1990), such as high-SiO₂ (58.81–69.02 wt.%), Al₂O₃ (15.01–17.94 wt.%), Na₂O (2.82–6.78 wt.%), Sr (433–1207 ppm), La (9.7–24.9 ppm) and low Y (4.8–12.6 ppm), Yb (0.4–1.17 ppm) and plot in the field of adakitic rocks with their high Sr/Y (35.2–246.2), chondrite-normalized La/Yb (10.9–48.8) ratios, and low Y contents and chondrite-normalized Yb values on the Sr/Y versus Y and chondrite-normalized (La/Yb)_N versus Yb the geochemical classification diagrams (Fig. 5A and B). In addition, the abundance of biotite, hornblende and plagioclase

within these rock groups supports the existence of an adakitic magma. On a total alkali-silica diagram (TAS), the studied adakitic rocks fall into mainly andesite and dacite fields with their moderate to high-SiO₂ contents (Fig. 6A). They belong to calc-alkaline and high-K calc-alkaline series on a K₂O versus SiO₂ diagram (Fig. 6B). However, on a Th-Co diagram (Hastie et al., 2007), which is particularly useful for altered and intensely weathered volcanic rocks, all the plots fall in the calc-alkaline field (Fig. 6C).

The second type of hornblende-rich andesites (Pirahmet andesite), which is well-exposed in the western part of the map area (Fig. 3), is geochemically distinguished from the first type of hornblende-rich andesites (Karakise Tepe andesite) with their high FeO^t (6.97–7.95 wt.%), Y (17.6–19.8 ppm) and low-SiO₂ (54.74–56.42 wt.%) contents (Table 3). These rocks show 0.55–0.64 wt.% TiO₂,

Table 4

Major, trace and rare earth element concentrations of non-adakitic basaltic-andesitic lithologies from the Kale area.

Sample	AH-1	AH-2	AH-3	AH-5	AH-6	AH-7	HT-70	HT-75	HT-82	HT-90	HT-91	HT-94	HT-96	HT-100	HT-108	HT-116	HT-117	HT-120	AH-11	AH-12
Rock type	Non-adakitic basalts and andesites (samples taken from fragments of agglomerate and volcanic breccia)															Basaltic andesite				
Level	Lower part						Middle part					Upper part				Dike				
Location	Kale															Yeniylol and Kale				
SiO ₂	49.22	48.33	48.58	47.44	48.88	47.44	50.64	51.34	51.25	51.66	52.86	52.99	53.72	53.14	54.55	52.08	52.87	50	51.03	53.16
TiO ₂	0.55	0.57	0.59	0.68	0.58	0.71	0.83	0.76	0.77	0.92	0.89	0.85	0.96	0.94	1.01	0.73	0.73	0.81	0.75	0.73
Al ₂ O ₃	18.71	18.96	19.16	18.56	19.41	17.62	18.69	21.37	19.47	19.07	18.39	18.01	15.13	16.81	15.26	19.75	19.63	19.18	20.64	19.83
Fe ₂ O ₃	6.85	6.85	7.29	8.87	7.79	9.74	9.13	7.69	9.25	9.97	8.96	8.74	9.4	9.63	9.71	8.37	8.35	10.44	8.55	8.36
MnO	0.15	0.16	0.16	0.17	0.15	0.19	0.16	0.13	0.07	0.16	0.18	0.13	0.14	0.14	0.14	0.16	0.16	0.18	0.17	0.17
MgO	3.35	3.37	3.49	4.39	4.09	5.38	3.85	2.45	3.75	3.75	3.01	3.57	3.06	3.12	2.75	3.08	3.04	4.84	3.21	3.11
CaO	9.45	10.12	9.59	9.28	9	9.08	9.38	8.67	9.04	9.24	8.51	7.79	6.19	6.4	5.68	9.12	8.8	10.02	8.96	8.85
Na ₂ O	2.97	2.91	2.91	2.69	2.58	2.39	3.09	3.72	3.33	2.98	3.68	3.31	4.54	4.51	4.65	3.11	3.31	2.7	3.61	3.41
K ₂ O	0.75	0.66	0.7	0.55	0.63	0.73	0.54	0.86	0.66	0.33	0.94	0.67	0.98	0.71	0.8	0.55	0.57	0.45	0.5	0.55
P ₂ O ₅	0.13	0.12	0.12	0.13	0.11	0.1	0.19	0.19	0.18	0.17	0.2	0.22	0.22	0.23	0.18	0.18	0.18	0.13	0.16	0.17
Cr ₂ O ₃	<0.002	<0.002	<0.002	<0.002	<0.002	0.002	<0.002	<0.002	<0.002	0.002	<0.002	<0.002	<0.002	0.002	<0.002	0.002	0.002	0.005	<0.002	<0.002
LOI	7.7	7.8	7.3	7.1	6.6	6.4	4.3	1.6	2	1.5	2.2	3.5	5.4	4.1	5	2.7	2.1	1	2.2	1.5
Total	99.83	99.85	99.89	99.86	99.82	99.78	99.8	99.78	99.77	99.75	99.82	99.78	99.74	99.73	99.73	99.83	99.74	99.76	99.78	99.84
Mg [#]	49.2	49.4	48.7	49.5	51.0	52.2	45.5	41.5	50.3	45.6	42.8	47.7	42.0	41.9	38.7	42.2	41.9	47.9	42.7	42.4
Na ₂ O + K ₂ O	3.72	3.57	3.61	3.24	3.21	3.12	3.63	4.58	3.99	3.31	4.62	3.98	5.52	5.22	5.45	3.66	3.88	3.15	4.11	3.96
Sc	18	18	19	25	21	31	29	24	25	27	27	21	22	21	23	23	23	34	23	23
V	153	157	169	220	171	252	264	233	253	269	242	199	192	191	237	195	197	302	189	187
Co	15	16	16.6	22.8	19.2	26.6	24.2	16.4	17	26.6	20.9	19.1	21	19.5	22.6	18.8	19.8	29	17.2	17.8
Ni	5.2	5.2	4.4	6.9	5.7	8.4	8.3	3.1	8.3	18.2	3.9	4.1	1.1	13.7	2.6	6.3	3	17	3.4	4
Cr																13.7	13.7	34.3		
Cu	43.9	44.2	42	43.8	36.6	39.5	118.4	381.6	42.6	77.3	72.6	25.3	17.9	15.2	13.1	98.3	134.1	133.8	125.4	143.7
Zn	40	41	41	44	44	53	52	31	44	38	39	36	35	51	39	46	42	38	38	36
Ga	13.4	12.7	14.1	15.3	13.7	14	17	18	16	18.1	17	16.4	12.7	13.9	13.3	16.5	16.1	16.9	15.6	15.5
Cs	0.3	0.3	0.2	0.3	0.3	0.2	0.1	0.2	0.2	1	0.3	0.2	0.7	0.7	1.2	0.1	0.1	0.1	<0.1	<0.1
Rb	13.8	11.6	12.3	9.6	8.9	12.1	4.6	13.5	11.5	25	21	10.2	20.6	15.6	16.8	5.4	5.2	4.5	5.5	5.6
Ba	383	306	295	215	173	215	227	322	266	235	350	277	375	321	306	209	228	158	242	221
Sr	497	486.8	450.7	437.8	602.9	390.4	532.2	541.4	512.1	473	433	470.8	809	912.5	784.3	538.5	539.1	419.1	523.1	505.6
Y	14.6	13.4	13.5	15.6	14.2	14.4	21.4	20.7	20.9	19.9	22.4	19.7	19.7	20.3	19.5	19.4	19	17.9	20	19.7
Zr	54.2	52.4	49.4	49.3	49	44.7	64.7	61	59.5	80.2	94.7	75.1	82.1	94.8	84.8	62.7	62.2	57.2	56	58.3
Nb	2.8	2.9	2.3	2.7	2.5	2.4	3.2	2.9	2.6	4.1	4.6	4.4	5.4	5.8	5.3	2.7	2.7	2.5	2.4	2.4
Hf	1.7	1.5	1.7	1.7	1.6	1.3	1.9	1.8	1.6	2.4	2.5	2.2	2.1	2.1	2.4	1.6	1.7	2	1.9	1.6
Ta	<0.1	<0.1	0.1	<0.1	0.1	0.1	0.1	0.1	0.2	0.2	0.3	0.2	0.2	0.3	0.3	0.1	0.1	0.1	0.1	0.1
Pb	4.4	4.4	3.8	3.8	3.8	3.4	3.3	3.8	1.9	1.7	3.3	2.2	4	4.3	5.2	4.4	3	1.6	5.3	3.1
Th	1.4	0.9	0.8	1	1.2	0.9	0.4	0.5	0.5	1.9	2.6	1.6	1.6	2.3	1.5	0.5	0.6	0.5	0.3	0.5
U	0.2	0.3	0.2	0.2	0.2	0.2	0.2	0.2	0.2	0.4	0.6	0.3	0.4	0.6	0.5	0.1	0.2	0.2	0.1	0.2
La	8.4	7.6	7.6	7.7	7.5	6.9	8.8	9.1	8.4	11.6	14.4	11.4	14.6	16.9	17.4	8.1	8	6.7	8	8.2
Ce	18.4	17	16.5	16.4	16.9	15.2	21.1	19.6	18.7	25.9	30.3	25.8	28.7	32.5	32.1	19.2	19.3	15.6	17.5	18.2
Pr	2.5	2.33	2.32	2.27	2.29	2.12	2.81	2.6	2.49	3.23	3.79	3.4	3.59	4.02	3.8	2.48	2.46	2.16	2.53	2.53
Nd	10.4	10.4	10.2	9.1	9.6	9.7	12.5	12.2	11.2	14	15.8	14.9	15.8	16.9	16.5	12.1	11.6	9.6	12.1	11.8
Sm	2.47	2.37	2.3	2.37	2.31	2.31	3.15	2.98	2.86	3.1	3.42	3.29	3.24	3.46	3.3	3.14	3.08	2.5	2.81	2.95
Eu	0.85	0.82	0.83	0.84	0.84	0.79	1.03	1.01	1.01	1.08	1.17	1.14	1.16	1.19	1.2	1.06	1.04	0.84	1.02	1
Gd	2.66	2.47	2.53	2.59	2.48	2.56	3.39	3.32	3.26	3.4	3.72	3.44	3.41	3.63	3.46	3.42	3.39	2.84	3.16	3.35
Tb	0.43	0.42	0.42	0.43	0.4	0.44	0.61	0.58	0.56	0.64	0.58	0.57	0.57	0.59	0.57	0.6	0.6	0.5	0.56	0.56
Dy	2.66	2.52	2.35	2.56	2.5	2.73	3.45	3.59	3.47	3.4	3.78	3.46	3.27	3.31	3.36	3.58	3.39	3.03	3.29	3.5
Ho	0.54	0.51	0.53	0.55	0.53	0.56	0.74	0.7	0.72	0.69	0.78	0.68	0.67	0.7	0.68	0.76	0.73	0.64	0.75	0.7
Er	1.57	1.51	1.56	1.65	1.53	1.65	2.1	2.13	2.22	2.09	2.34	2.1	1.98	2.09	2.06	2.17	2.17	1.92	2.14	2.09
Tm	0.25	0.23	0.23	0.24	0.23	0.26	0.33	0.34	0.35	0.33	0.36	0.31	0.31	0.31	0.31	0.36	0.32	0.29	0.33	0.34
Yb	1.55	1.53	1.5	1.62	1.49	1.59	2.03	2.06	2.25	1.95	2.2	1.98	1.92	2.01	1.87	2.25	2.2	1.84	2.07	2.1
Lu	0.24	0.23	0.24	0.24	0.24	0.24	0.33	0.33	0.35	0.31	0.34	0.31	0.3	0.32	0.3	0.32	0.33	0.29	0.33	0.32

Table 4 (continued)

Sample	AH-1	AH-2	AH-3	AH-5	AH-6	AH-7	HT-70	HT-75	HT-82	HT-90	HT-91	HT-94	HT-96	HT-100	HT-108	HT-116	HT-117	HT-120	AH-11	AH-12
Rock type	Non-adakitic basalts and andesites (samples taken from fragments of agglomerate and volcanic breccia)																			
Level	Lower part				Middle part								Upper part				Basaltic andesite			
Location	Kale												Dike				Yeniyoil and Kale			
Sr/Y	34.0	36.3	33.4	28.1	42.5	27.1	24.9	26.2	24.5	23.8	19.3	23.9	41.1	45.0	40.2	27.8	28.4	23.4	26.2	25.7
(La/Yb) _N	3.7	3.3	3.4	3.2	3.4	2.9	2.9	3.0	2.5	4.0	4.4	3.9	5.1	5.7	6.3	2.4	2.5	2.5	2.6	2.6

17.58–17.94 wt.% Al_2O_3 , 2.92–3.65 wt.% MgO , 3.42–4.36 wt.% Na_2O , 5.16–6.31 wt.% CaO , 0.83–1.64 wt.% K_2O , 2–4.3 ppm Ni, 21.3–41.3 ppm Rb, 421–473 ppm Sr, 72–124 ppm Zr, 12.6–18.4 ppm La and 1.94–2.08 ppm Yb (Table 3). Mg numbers range from 45.2 to 48. The agglomerate and volcanic breccia clasts collected from the pyroclastic sequence of the Alibaba Formation have 47.44–54.55 wt.% SiO_2 , 0.55–1.01 wt.% TiO_2 , 15.26–21.37 wt.% Al_2O_3 , 6.85–9.97 wt.% Fe_2O_3 , 2.45–5.38 wt.% MgO , 5.68–10.12 wt.% CaO , 2.39–4.65 wt.% Na_2O and 0.55–0.98 wt.% K_2O (Table 4). Their Sr and Y concentrations are 390–913 ppm and 13.6–22.4 ppm, respectively. Both hornblende-rich andesites (Pirahmet andesite) and agglomerate-volcanic breccia clasts fall into the non-adakitic rock field with their relatively high Y (13–23 ppm) contents and chondrite-normalized Yb (7.7–10.8) values on the Sr/Y versus Y and chondrite-normalized (La/Yb)_N versus Yb diagrams (Fig. 5A and B). The non-adakitic basaltic rocks representing the final stage of the Cenozoic magmatism in the study area are slightly different from the other non-adakitic lithologies with their relatively high- Al_2O_3 (19.63–20.64 wt.%) and low Rb (4.5–5.6 ppm) contents (Table 4). The studied non-adakitic rocks plot in the subalkaline basalt, basaltic andesite and andesite fields on a total alkali-silica diagram (Fig. 6A). On K_2O versus SiO_2 and Th versus Co geochemical classification diagrams, they fall in calc-alkaline field, except for a few samples (Fig. 6B and C).

5. Results and discussion

5.1. Timing of adakitic and non-adakitic magmatism

In the study area, the biotite-rich adakitic andesites (Kizil Tepe andesite) show intrusive contact with the early-mid-Jurassic Zimonköy Formation, the late Jurassic–early Cretaceous Berdiga Formation and the late Cretaceous Kermutdere Formation (Figs. 3 and 4A). The hornblende-rich adakitic andesites (Karakise Tepe andesite) cut the late Cretaceous sediments and is overlain by a massive-middle bedded, yellowish brown colored, nummulite-bearing limestone around the Karakise Hill (Figs. 3 and 4C). Similarly, the Kircaova dacite has a sharp intrusive contact with the monogenic conglomerates consisting of the basement of the late Cretaceous Kermutdere Formation in the south of Kale village (Fig. 3). The hyaloclastic breccia, covers the nummulite-bearing limestones representing the basement of the early Cenozoic Alibaba Formation, exposed immediately north of the Kale village (Figs. 3 and 4F). These field observations and stratigraphic relations indicate a Paleocene–Eocene age for the adakitic activity in the study area. The adakitic magmatism was followed by the non-adakitic basaltic-andesitic magmatism which is widely distributed at the northern part of the Gumushane–Bayburt–İspir line in the eastern Pontides orogenic belt. Kaygusuz et al. (2011) suggested that the early Cenozoic non-adakitic basaltic-andesitic magmatism occurred between 44 (± 2.59) and 33.45 (± 2.32) Ma, based on K–Ar ages obtained from hornblende within andesitic rocks exposed in Torul (Gumushane) area. However, these basaltic-andesitic lithologies are cut by the non-adakitic Lutetian (48–40 Ma) granitic rocks in the Gumushane (Karsli et al., 2007) and Bayburt–Aydintepe (Eyuboglu et al., 2011a) areas. Therefore, the age span given by Kaygusuz et al. (2011) for the early Cenozoic non-adakitic basaltic-andesitic magmatism in the Gumushane area is contradictory.

In order to determine the precise timing of the early Cenozoic magmatism in the study area, zircons from two andesite samples representing adakitic (AR-1) and non-adakitic magmatism (HT-100) were dated by LA-ICP-MS method at the National Taiwan University. The analytical procedures for LA-ICP-MS technique were same as those described in Chiu et al. (2009) and Eyuboglu et al. (2011f).

The majority of zircons extracted from the biotite-rich adakitic andesite (sample AR-1) display euhedral crystal morphology with

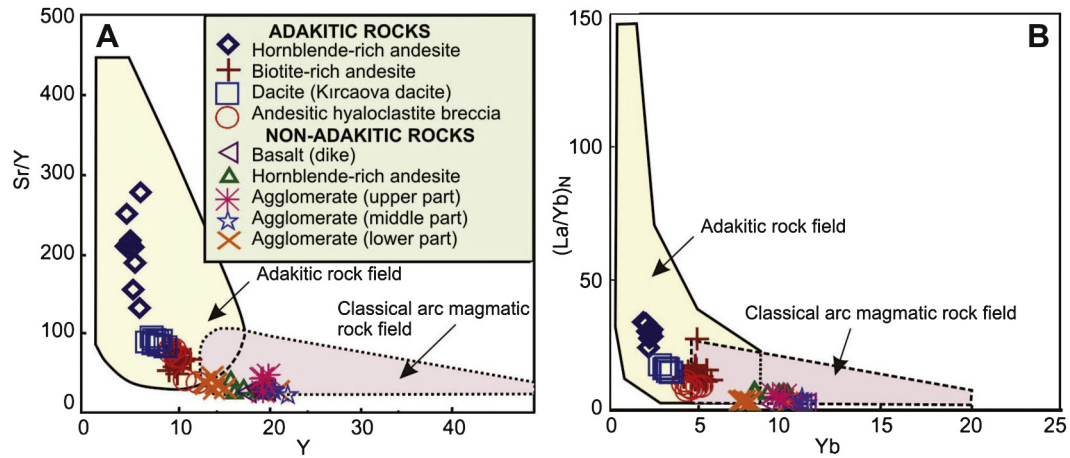


Figure 5. Y versus Sr/Y (A) and Yb versus (La/Yb)_N (B) geochemical classification diagrams for the studied early Cenozoic Kale magmatic rocks (after Defant and Drummond, 1990).

oscillatory core typical of zircons crystallized from magmas. Their Th/U ratios range from 0.46 to 1.2 (Table 5). These high values are consistent with a magmatic origin (Rubatto, 2002). U-Pb determinations of thirteen zircon grains from the sample AR-1 yielded $^{206}\text{Pb}/^{238}\text{U}$ ages from 46 to 50 Ma, with a weighted mean age of 48.71 ± 0.74 Ma (Fig. 7A). In addition, in a recent study (Aslan, 2010), U-Pb zircon age of 46 Ma was reported from the adakitic tuffs exposed at about 30 km west of the study area. Both zircon ages are concordant with our field observations and indicate that

the adakitic activity prevailed between 49 and 46 Ma in the Gumushane area.

The euhedral zircon grains extracted from a non-adakitic andesite from the upper part of the Alibaba Formation exhibit oscillatory zoning typical of zircons that crystallized from a magma. In addition, they have high Th/U ratios between 0.60 and 1.08 (Table 5), supporting a magmatic origin during their evolution (Rubatto, 2002). Sixteen zircons from the non-adakitic andesite gave ages of 41–47 Ma, with a weighted mean age of 44.68 ± 0.84 Ma

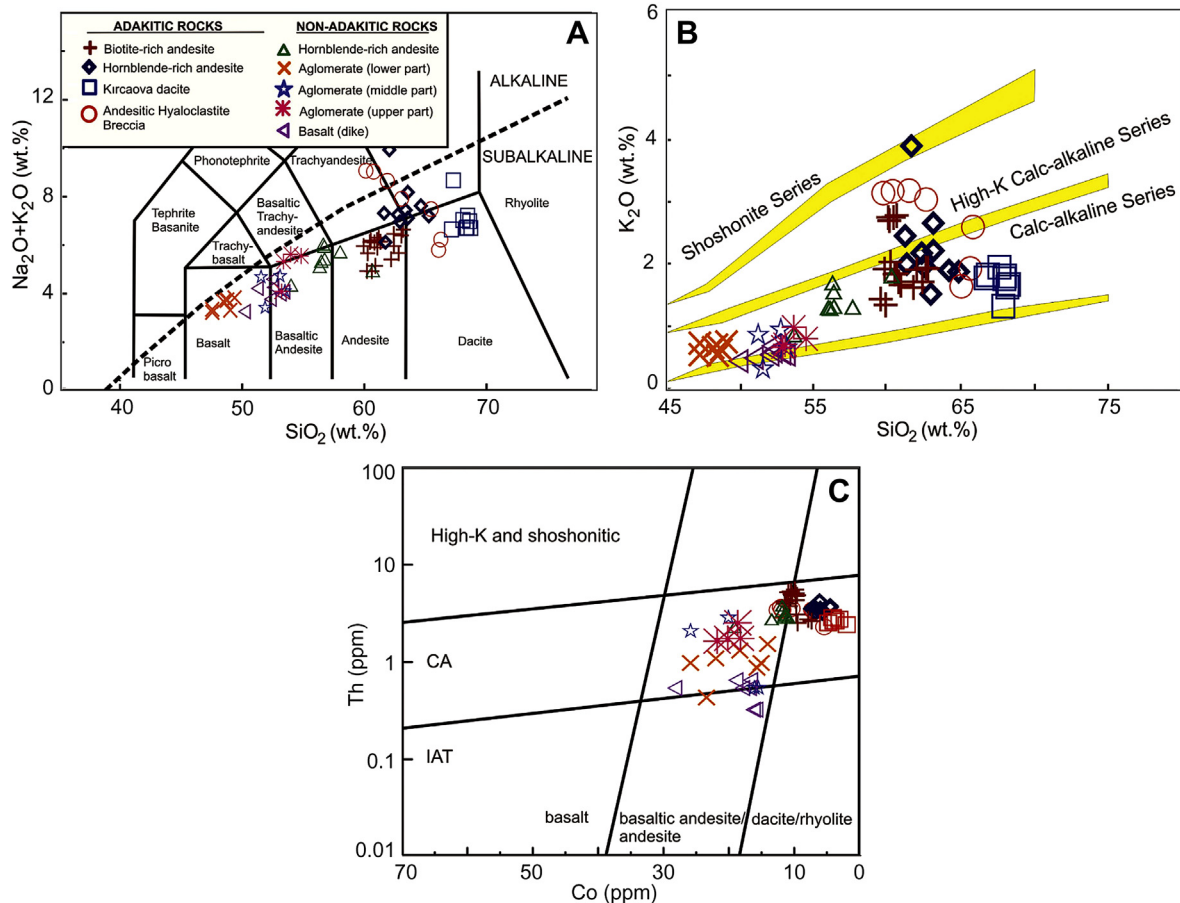


Figure 6. SiO₂ versus total alkali (A) and K₂O (B) and Co versus Th (C) diagrams for the Kale adakitic and non-adakitic rocks (A: after Le Bas et al., 1986; B: after Rickwood, 1989; C: after Hastie et al., 2007).

Table 5

U–Pb LA-ICP-MS analytical data of zircon crystals from a biotite-rich adakitic andesite (AR-1) and a non-adakitic andesite (HT-100) from the Kale area.

Spot	U (ppm)	Th/U	U-Th-Pb ratios								Ages (Ma)							
			²⁰⁷ Pb/ ²³⁵ U	±1σ	²⁰⁶ Pb/ ²³⁸ U	±1σ	²⁰⁷ Pb/ ²⁰⁶ Pb	±1σ	²⁰⁸ Pb/ ²³² Th	±1σ	²⁰⁶ Pb/ ²³⁸ U	±1σ	²⁰⁷ Pb/ ²⁰⁶ Pb	±1σ	²⁰⁷ Pb/ ²³⁵ U	±1σ	²⁰⁸ Pb/ ²³² Th	±1σ
Biotite-rich adakitic andesite (sample no: AR-1)																		
AR1-02	507	0.48	0.0514	0.0019	0.0077	0.0002	0.0483	0.0010	0.0025	0.0001	50	1	112	48	51	2	50	1
AR1-04	247	0.46	0.0506	0.0029	0.0078	0.0002	0.0469	0.0018	0.0025	0.0001	50	1	44	83	50	3	51	2
AR1-05	513	0.52	0.0482	0.0023	0.0076	0.0002	0.0461	0.0015	0.0025	0.0001	49	1	3	66	48	2	50	1
AR1-06	112	1.20	0.0462	0.0054	0.0077	0.0002	0.0438	0.0042	0.0024	0.0001	49	1	−81	189	46	5	48	2
AR1-08	763	0.78	0.0495	0.0015	0.0077	0.0002	0.0470	0.0008	0.0023	0.0001	49.1	1	47	36	49	1	47	1
AR1-09	610	0.93	0.0475	0.0017	0.0075	0.0002	0.0460	0.0009	0.0023	0.0001	48.1	1	−5	35	47	2	46	1
AR1-10	419	0.43	0.0501	0.0021	0.0078	0.0002	0.0467	0.0011	0.0026	0.0001	50	1	33	52	50	2	53	2
AR1-11	528	0.67	0.0471	0.0028	0.0072	0.0001	0.0476	0.0022	0.0023	0.0001	46.1	0.9	80	106	47	3	46	1
AR1-12	357	0.47	0.0501	0.0022	0.0075	0.0002	0.0481	0.0013	0.0025	0.0001	48	1	106	57	50	2	49	1
AR1-14	634	0.76	0.0451	0.0016	0.0074	0.0002	0.0442	0.0009	0.0023	0.0001	47.5	1	−59	40	45	2	46	1
AR1-14C	278	0.50	0.0504	0.0028	0.0075	0.0002	0.0490	0.0018	0.0024	0.0001	48	1	146	86	50	3	48	2
AR1-18	527	0.49	0.0503	0.0019	0.0077	0.0002	0.0471	0.0010	0.0026	0.0001	50	1	56	47	50	2	52	2
AR1-20	503	0.81	0.0534	0.0048	0.0077	0.0002	0.0504	0.0036	0.0024	0.0000	49	1	215	169	53	5	48.9	0.9
Non-adakitic andesite (sample no: HT-100)																		
HT-02	130	0.96	0.0439	0.0037	0.0069	0.0002	0.0461	0.0032	0.0023	0.0001	44	1	2	140	44	4	45	2
HT-03	111	0.61	0.0438	0.0052	0.0068	0.0002	0.0469	0.0047	0.0022	0.0001	43	1	42	202	43	5	44	2
HT-04	216	0.89	0.0451	0.0035	0.0071	0.0002	0.0461	0.0029	0.0023	0.0001	46	1	4	129	45	3	46	1
HT-05	219	1.08	0.0410	0.0029	0.0065	0.0002	0.0461	0.0026	0.0021	0.0001	41.4	0.9	2	115	41	3	43	2
HT-06	237	0.88	0.0427	0.0028	0.0070	0.0002	0.0441	0.0020	0.0024	0.0001	45	1	−66	90	42	3	48	2
HT-08	125	0.87	0.0438	0.0057	0.0068	0.0002	0.0470	0.0051	0.0022	0.0001	43	1	48	237	44	6	43	2
HT-09	167	0.92	0.0541	0.0045	0.0073	0.0002	0.0536	0.0032	0.0027	0.0001	47	1	354	134	54	4	53	2
HT-11	145	0.79	0.0526	0.0046	0.0070	0.0002	0.0548	0.0036	0.0027	0.0001	45	1	403	145	52	4	53	2
HT-11	82	0.64	0.0428	0.0153	0.0065	0.0003	0.0476	0.0154	0.0021	0.0004	42	2	80	557	43	15	42	8
HT-14	283	0.85	0.0484	0.0027	0.0070	0.0002	0.0504	0.0018	0.0024	0.0001	45	1	212	76	48	3	47	2
HT-15	210	0.87	0.0447	0.0044	0.0070	0.0002	0.0464	0.0038	0.0022	0.0001	45	1	20	181	44	4	45	2
HT-16	349	0.89	0.0453	0.0037	0.0071	0.0002	0.0462	0.0031	0.0023	0.0001	46	1	6	142	45	4	46	1
HT-17	148	0.81	0.0431	0.0038	0.0068	0.0002	0.0461	0.0033	0.0023	0.0001	44	1	1	168	43	4	46	2
HT-18	106	0.78	0.0699	0.0060	0.0069	0.0002	0.0738	0.0045	0.0024	0.0001	44	1	1035	121	69	6	48	2
HT-19	126	0.60	0.0455	0.0036	0.0072	0.0002	0.0461	0.0029	0.0024	0.0002	46	1	1	122	45	4	48	3
HT-20	280	0.64	0.0436	0.0030	0.0069	0.0002	0.0461	0.0025	0.0022	0.0001	44	1	4	116	43	3	45	2

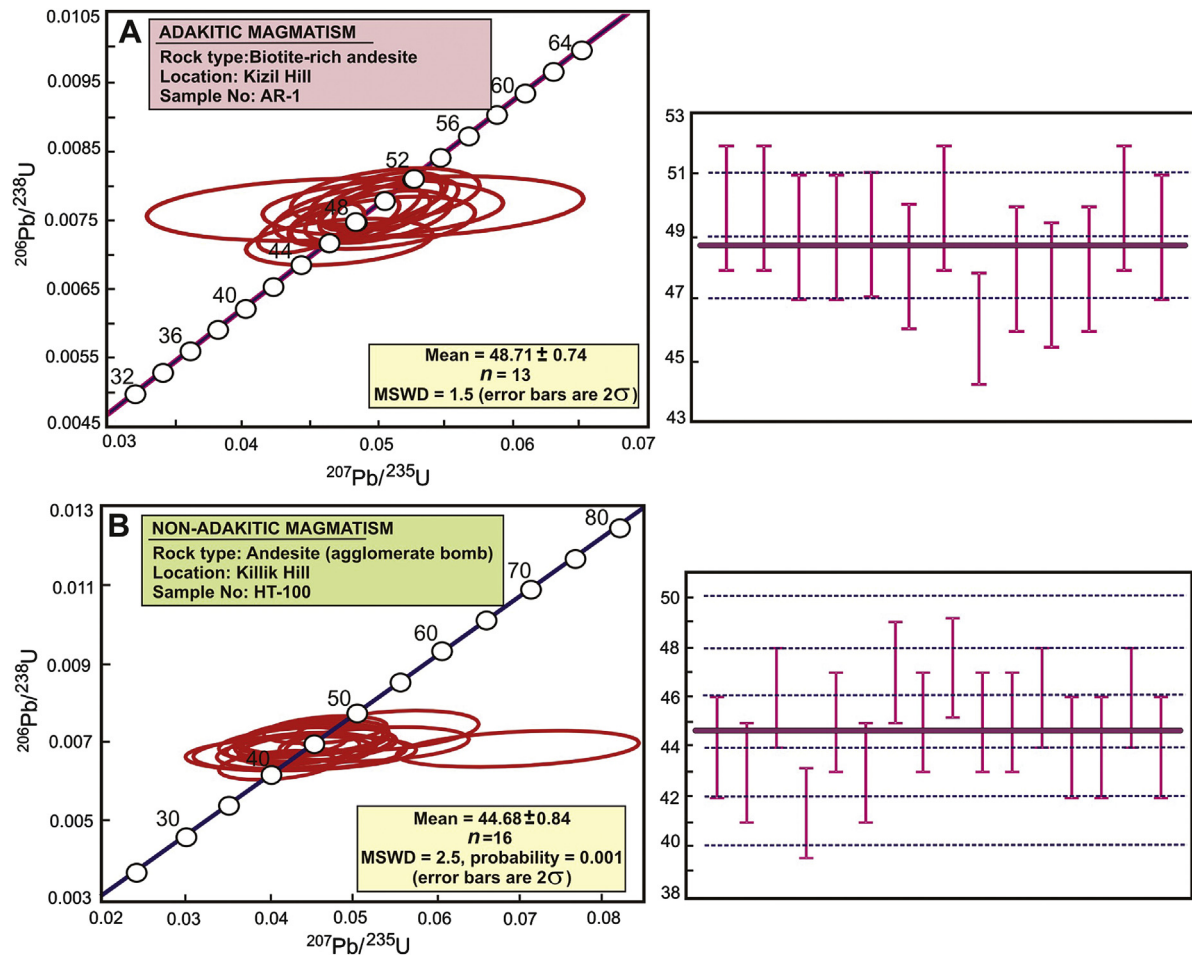


Figure 7. Concordia diagrams of zircons from Kale adakitic (A) and non-adakitic (B) rocks.

(Fig. 7B). This age is consistent with our field observations and confirms that there is no significant time gap in the magmatic activity during the transition from adakitic to non-adakitic basaltic-andesitic magmatism in the Gumushane area.

5.2. Petrogenesis

5.2.1. The origin of the adakitic magmatism

In the Aleutian chain of Alaska, Kay (1978) recognized a distinctive rock type, a magnesian andesite, different from the normal arc magmas and suggested that the rock was generated by partial melting of the garnet- and clinopyroxene-rich, basaltic portion of the subducted Pacific oceanic crust. This geochemically distinctive group of andesite and dacites, characterized by high-SiO₂ (>56 wt.%), Al₂O₃ (>15 wt.%), Na₂O (>3.5 wt.%), Sr/Y (>40) and La/Yb (>20), and low HFSE (high field strength elements), was originally termed as 'adakite' and interpreted as a product of partial melting of hot, young (<25 Ma) subducted oceanic crust by Defant and Drummond (1990). Subsequent investigations led to several discussions and debates on the origin of adakitic rocks. Atherton and Petford (1993) proposed an alternative model where adakites were considered to be products of partial melting of newly underplated basaltic crust. According to Sajona et al. (1993), melting of a MORB (mid oceanic ridge basalt) component of the subducting slab followed by garnet fractionation is responsible for their unusual trace element concentrations. Feeley and Hacker (1995) suggested that contamination of mantle-derived basaltic magmas in garnet-bearing mafic continental crust is an alternative mechanism to

slab-melting to produce the early Archean TTG (tonalite-trondhjemite-granodiorite) suites and younger rocks with similar compositions. Shimoda et al. (1998) emphasized that the Setouchi high-Mg andesites with adakitic signatures include components which suggest derivation from partial melting of sediments on the subducted plate. According to Castillo et al. (1999), the Mindanao adakites are not pure basaltic crust melts and are products of an assimilation and fractional crystallization (AFC) process with negligible connection to melting of subducted basaltic crust. By 2000s, the petrology, classification and geotectonic setting of adakitic rocks have received considerable attention. Whereas some authors suggested that the adakitic rocks were generated by delamination or partial melting of thickened continental crust after collisional orogeny (e.g., Xu et al., 2002; Chung et al., 2003; Gao et al., 2004; Guo et al., 2006; Wang et al., 2005, 2006a,b), others proposed a slab window formation related to ridge subduction (e.g., Kinoshita, 2002; Thorkelson and Breitsprecher, 2005; Rodriguez et al., 2007; Santosh et al., 2009; Santosh and Kusky, 2010; Zhang et al., 2010; Eyuboglu et al., 2011a,b,c,d). Martin et al. (2005) divided adakites into two subgroups as high silica adakites related to slab melts and low silica adakites representing products of metasomatized mantle. Adakites have been documented from about half of the active volcanic arcs (Martin, 1998) and occur in various hot subduction settings, including active ridge subduction (Lagabrielle et al., 2000), subduction of very young (<5 Ma) oceanic crust (Sajona et al., 1993; Peacock et al., 1994), and flat slab subduction (Gutscher et al., 2000). These different hypotheses on the petrogenesis and geodynamic setting of the adakitic rocks

indicate that their chemistry is not a robust criteria in interpreting of their origin and geodynamic setting.

The primitive mantle-normalized trace element abundance patterns of the adakitic rocks investigated in this study display strong enrichment in large ion lithophile elements (LILE) relative to high field strength elements (HFSE) and negative Nb, Ta, P, Zr, Ti anomalies (Fig. 8A), suggesting a similar origin to those of subduction-related arc magmatics. The chondrite-normalized rare earth element patterns for the Kale adakitic rocks exhibit a steep decrease from light rare earth elements (LREE) to heavy rare earth elements (HREE), and typically lack Eu anomalies (Fig. 8B). In the studied adakitic rocks, the low Y and HREE is caused either by melting in the presence of garnet, or fractionation of garnet (=high-pressure process), whereas the process of enrichment of Sr and similar elements is likely to result through the introduction of an enriched fluid phase (silicate melt or hydrous fluid) at any stage in the evolution of the melt (Eyuboglu et al., 2012). In addition, their low Yb contents (<1.17 ppm) are consistent with subduction-related rocks produced at mantle depths (Bourdon et al., 2002). The Seme adakitic rocks from the eastern Pontides orogenic belt, which are exposed ca. 70 km southwest of the study area, reveal remarkable negative trends in nearly all major, trace and rare earth elements with increasing SiO₂ content, suggesting a high-pressure fractional crystallization process for their origin (Eyuboglu et al., 2011c). On the Harker variation diagrams (Fig. 9), trace and rare earth element concentrations of the Kale adakitic rocks do not exhibit negative correlations with increasing SiO₂ as in Seme adakitic rocks, suggesting that a high-pressure fractional crystallization did not play an important role in their petrogenesis (Fig. 9). However, major element variation diagrams show a negative correlation for FeO^t, MgO, CaO and K₂O, while Na₂O and Al₂O₃ display a slightly positive correlation with SiO₂ (Fig. 9). These positive and negative anomalies might be related to the low-pressure fractional crystallization of the Kale adakitic magmas.

The Kale adakitic rocks do not show any conspicuous Eu anomaly (Fig. 8B), which suggest that plagioclase was not a major phase controlling the fractional crystallization and/or accumulation during their evolution. In the magmatic systems, the nature of Eu

anomaly has been explained in three ways. The first is that plagioclase does not control the Eu distribution during either partial melting or fractional crystallization; either plagioclase is absent (high-pressure melting or crystallization) or some other phase dominates the Eu budget. The second alternative is elevated oxygen fugacity during the melting or crystallization process, such that Eu²⁺ is minimized, Eu³⁺ is dominant in the system, and the D_{Eu} is consistent with D_{Sm} and D_{Tb} ; this is partly also linked to plagioclase composition. The Eu anomaly associated with plagioclase gets smaller as the plagioclase composition becomes more Ca-rich. The third possibility is that a specific mineral assemblage (usually a combination of plagioclase and amphibole, or plagioclase, amphibole and apatite) was involved in fractionation or melting, such that the bulk D_{Eu} is similar to bulk D_{Sm} and D_{Tb} , leading to the absence of anomaly. The presence of plagioclase in the studied rocks does not necessarily mean that an Eu anomaly will be present – it simply means that plagioclase crystallized at a time when its Eu content did not modify the bulk rock REE pattern.

Eyuboglu et al. (2011f) argued that the Cenozoic adakitic activity in the eastern Pontides orogenic belt occurred in two different cycles during the late Paleocene–early Eocene and the late Miocene. The debate on the origin of the late Paleocene–early Eocene adakitic rocks still continues. Some authors suggest that they were generated by partial melting and/or delamination of thickened arc crust after the collision between Tauride and Pontide blocks (Dilek et al., 2010; Karlı et al., 2010; Eyuboglu et al., 2011a,b,c,d,e; Topuz et al., 2011). However, based on systematic geological, geochemical and geochronological data obtained from the whole region, Eyuboglu et al. (2011a,b,c,d,e) suggest that the generation of the eastern Pontides early Cenozoic adakitic magmas is a result of the ridge subduction-related slab window formation and simultaneously slab roll-back processes in a south-dipping subduction zone. The late Miocene adakitic rocks are exposed in a limited area covering the southeastern part of the eastern Pontides orogenic belt and south of the Lesser Caucasus and their origin is related to the late Miocene partial melting of thickened mafic lower continental crust after the collision between Greater Caucasus and Lesser Caucasus during Oligo-Miocene time (Eyuboglu et al., 2012). The

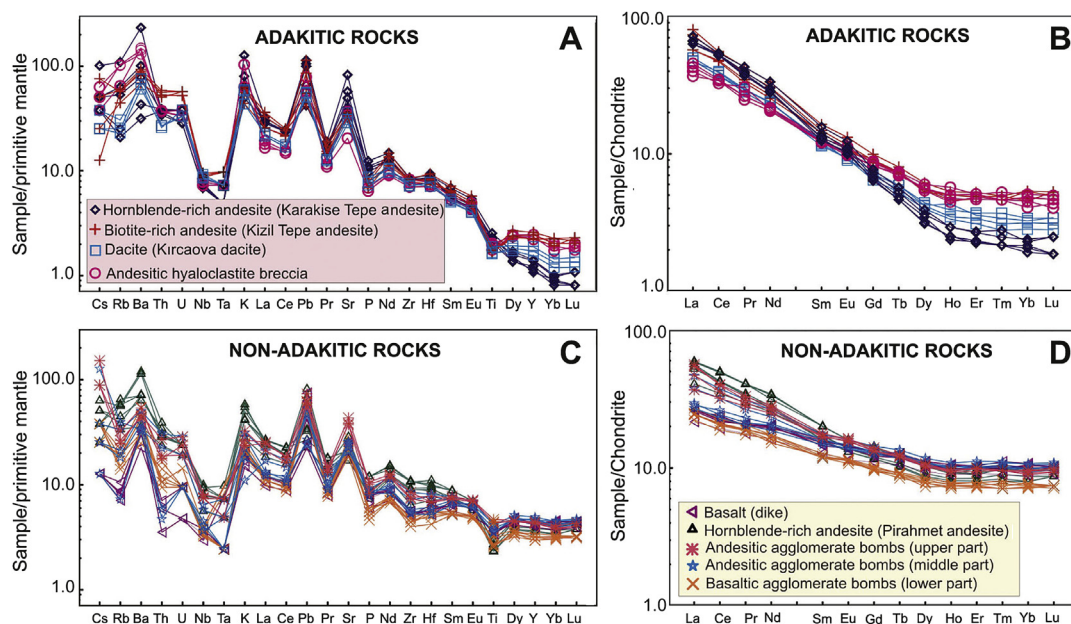


Figure 8. Primitive mantle-normalized trace element (A and C) and chondrite-normalized rare earth element (B and D) distribution patterns for the Kale adakitic and non-adakitic rocks (primitive mantle values: Sun and McDonough, 1989; chondrite values: Boynton, 1984).

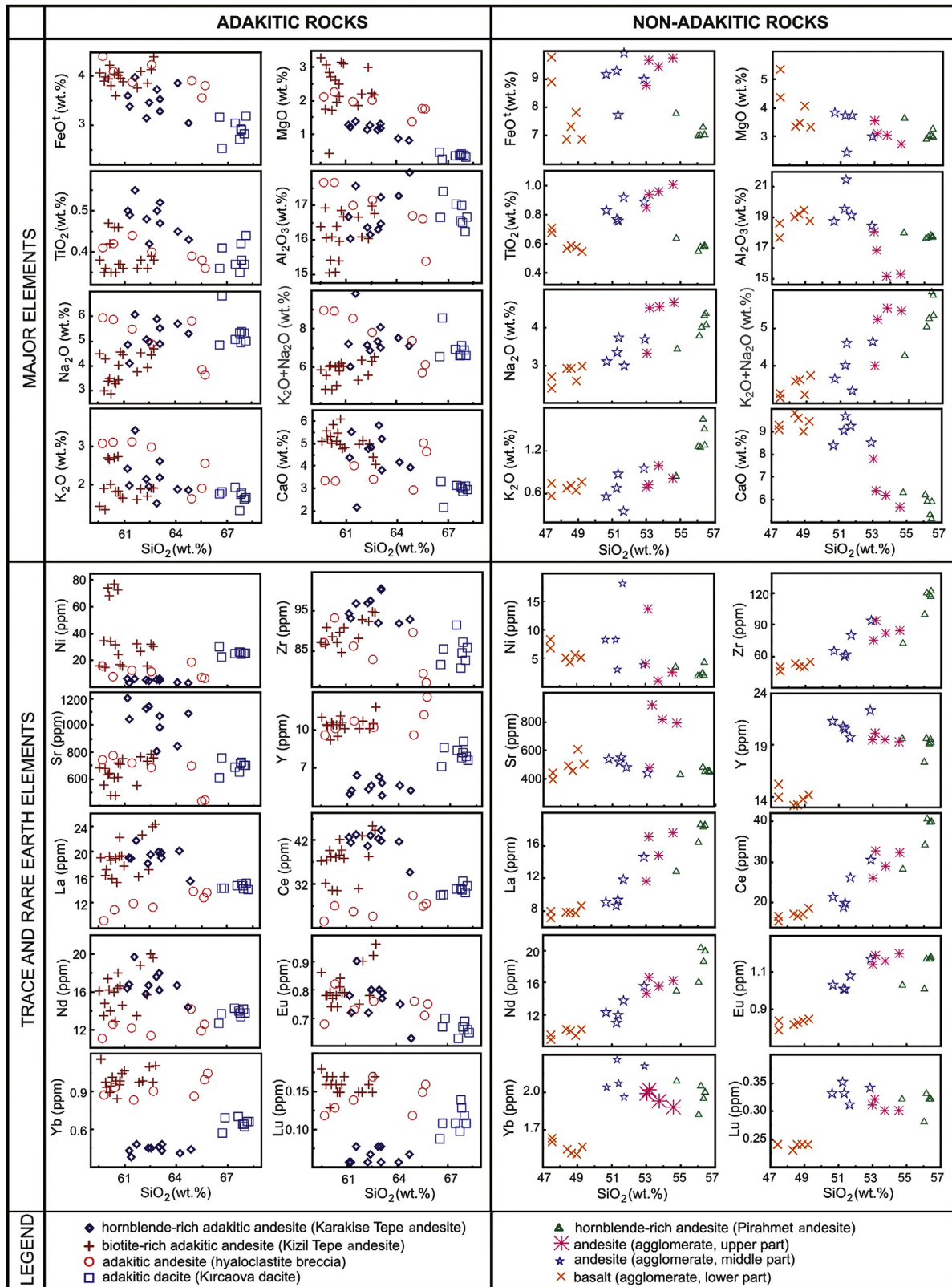


Figure 9. Harker variation diagrams for the studied adakitic and non-adakitic rocks.

studied early Eocene adakitic rocks are different from crust-derived the late Miocene adakites with their high Nb/Ta and low Zr/Sm values and are plot in the fields of the oceanic slab-derived and/or slab window-related adakitic rocks on a Nb/Ta versus Zr/Sm

diagram (Fig. 10A). Similarly, their low Th/La and Th values are consistent with the subducted oceanic slab-derived and/or slab window-related adakitic rocks, rather than thickened arc crust or subducted continental crust-derived adakitic rocks (Fig. 10B). The

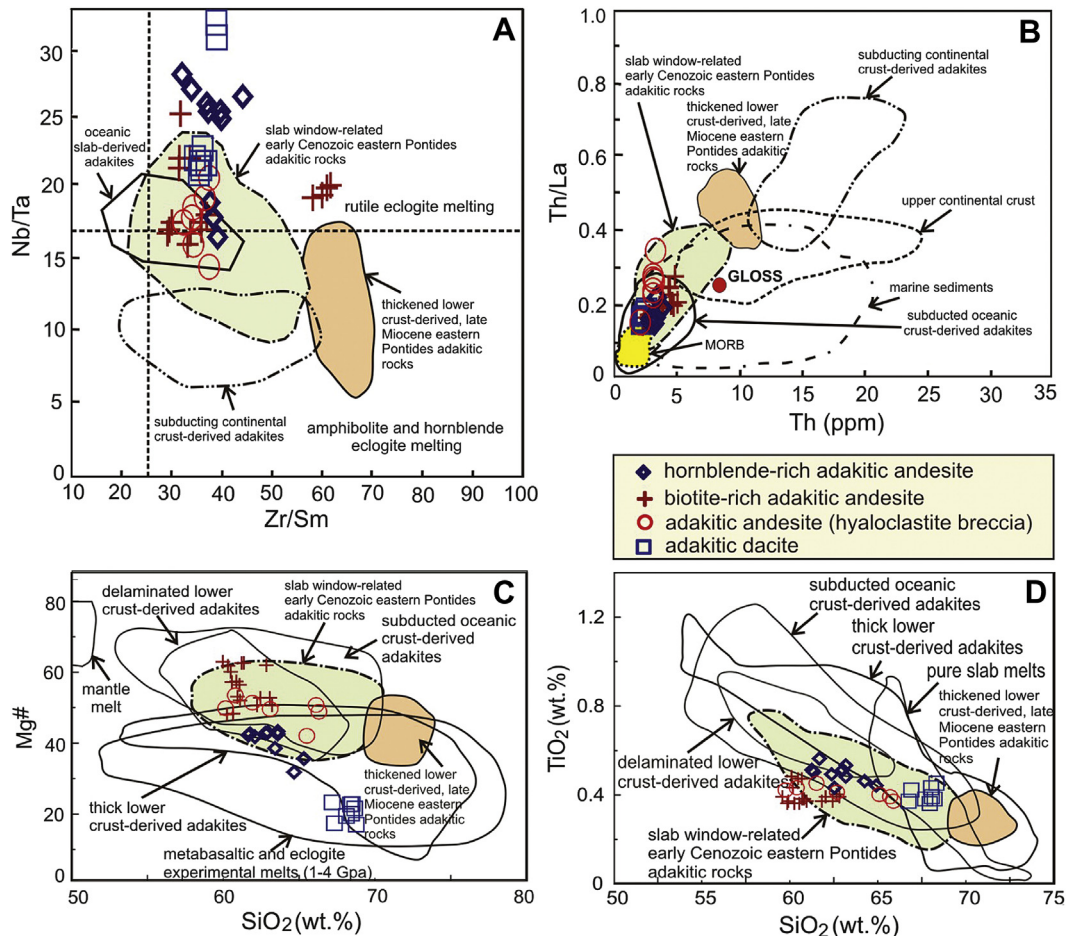


Figure 10. Zr/Sm versus Nb/Ta (A), Th versus Th/La (B), and SiO₂ versus Mg[#] and TiO₂ (C and D) diagrams for the early Cenozoic Kale adakitic and non-adakitic rocks. (A): The fields of oceanic slab-derived and subducting continental crust-derived are after [Condie \(2005\)](#) and [Wang et al. \(2004\)](#), respectively. The data for slab window-related and thickened-lower crust-derived adakites are after [Eyuboglu et al. \(2011a\)](#) and [Eyuboglu et al. \(2012\)](#), respectively; (B): The data for marine sediments and upper continental crust are from [Plank and Langmuir \(1998\)](#) and [Condie \(1993\)](#), respectively. The field of subducted oceanic crust-derived adakites is after [Defant et al. \(2002\)](#) and [Martin et al. \(2005\)](#); (C and D): Subducted oceanic crust-derived adakites ([Wang et al., 2006a](#)), delaminated lower crust-derived adakites ([Xu et al., 2002](#); [Gao et al., 2004](#); [Wang et al., 2004, 2006a, b](#)), pure slab melts ([Stern and Kilian, 1996](#)), metabasaltic and eclogite experimental melts ([Rapp et al., 1999, 2002](#)), thick lower crust-derived adakites ([Atherton and Petford, 1993](#); [Muir et al., 1995](#); [Petford and Atherton, 1996](#); [Johnson et al., 1997](#)).

Kale adakitic rocks generally display a wide range of SiO₂ (58–69 wt.%) and Mg[#] (17–62) and plot in the fields of subducted oceanic slab-derived and/or slab window-related adakitic rocks on a Mg[#] versus SiO₂ diagram, except for Kircaova dacite ([Fig. 10C](#)). However, on a TiO₂ versus SiO₂ diagram ([Fig. 10D](#)), all of the studied adakitic rocks fall into the slab-derived and/or slab window-related adakitic rock field. When considering into both field data and the negative correlation of Mg[#] and FeO^t with increasing SiO₂ ([Figs. 9 and 10C](#)), we suggest that the dacitic rocks of Kircaova represent the final stage of the adakitic activity in the study area and they were formed by low-pressure fractionation of andesitic parental magma.

[Guo et al. \(2006\)](#) classified the late Mesozoic Sulu adakitic rocks into two subgroups as low- and high-Al andesites. The low-Al adakitic andesites formed as part of the eclogitic lower continental crust delaminated and the melts from that sinking slab ascended through the lithospheric mantle and reacted with peridotites. Whereas the high-Al adakitic andesite series were generated by melting of the lower portion of eclogitic crust that remained after the delamination event, without any interaction with mantle peridotite. By using a model identical to the one proposed by [Guo et al. \(2006\)](#), [Karlı et al. \(2010\)](#) suggested that the eastern Pontides Kale adakitic rocks were generated by delamination of thickened-lower

continental crust after the emplacement onto Pontide block of the Tauride block based on the collision between Pontide and Tauride blocks in the south of the magmatic arc during the Paleocene. However, the geological characteristics of the Sulu belt and the eastern Pontides orogenic belt are very different from each other. Detailed field studies indicate that a belt including mafic-ultramafic massifs are exposed along the entire belt between eastern Pontides and Taurides and there is no any location where the Tauride platform rests on the eastern Pontides magmatic arc ([Bektaş et al., 1995, 1999](#); [Eyuboglu et al., 2011a,b,c,d,e](#); [Fig. 1](#)). Without exception, all of the adakitic intrusions in the study area occur within the autochthonous units of the eastern Pontides orogenic belt. In addition, our systematic geochronological studies indicated that the adakitic magmatism migrated toward north in time ([Eyuboglu et al., 2011a,b,c,d,e](#)). This northward migration of adakitic activity in the eastern Pontides orogenic belt cannot be explained by the partial melting and/or delamination of thickened arc lower crust. According to [Eyuboglu et al. \(2011a,b\)](#), the progressively younging of early Cenozoic adakitic activity toward the north indicates that the eastern Pontides early Cenozoic adakitic rocks were generated in a slab window related to ridge subduction ([Eyuboglu et al., 2011a,b](#)). Moreover, the late Paleocene–early Eocene adakites are well-exposed in the south of the eastern Pontides orogenic belt. But

they don't appear in the western Pontides and Caucasus. This limited distribution of early Cenozoic adakitic rocks along the Pontides–Caucasus belt also supports a slab window model for their origin (Eyuboglu et al., 2011a,b,c,d,e).

5.2.2. The origin of the non-adakitic magmatism

The active continental margins are the most important sites of magma generation in the ancient and modern plate convergence systems. In these areas, the various magmatic processes such as crystal fractionation, assimilation of crustal material by basaltic magma and magma mixing play a very important role in the petrogenetic evolution of adakitic and/or non-adakitic calc-alkaline magmas (e.g., Gao et al., 2012; Guan et al., 2012; Qi et al., 2012).

In the study area, non-adakitic igneous suite is represented by the calc-alkaline basaltic-andesitic volcanic rocks and their pyroclastic equivalents. The primitive mantle-normalized trace element distribution patterns of the studied non-adakitic rocks exhibit enrichment in large ion lithophile (LIL) elements relative to high field strength (HFS) elements and also negative Nb, Ta, Zr and Ti anomalies, suggesting a subduction-related origin in their petrogenesis (Fig. 8C). Chondrite-normalized rare earth element patterns for the studied rocks show light rare earth (LRE) element enrichment with respect to heavy rare earth (HRE) elements, with no significant Eu anomalies (Fig. 8D). When compared with the Kale adakitic rocks, their low $(La/Yb)_N$ values ranging from 2.4 to 6.3 are consistent with the separation from garnet-poor residues at shallower depth. The lacking of any conspicuous positive or negative Eu anomaly indicates that neither plagioclase fractionation nor melting to leave plagioclase-bearing residues were important in generation of non-adakitic basaltic-andesitic magmas in the Kale area. The strong negative P anomaly reflects apatite fractionation (Fig. 8C). On the Harker variation diagrams (Fig. 9), Na_2O , K_2O , Zr and LRE elements (La, Ce, Nd, Eu) are positively correlated with SiO_2 whereas MgO , CaO and Ni are negatively correlated, suggesting that fractional crystallization was a key process in petrogenetic evolution of the Kale non-adakitic magmas. During the fractional crystallization of a basaltic magma, early-formed minerals such as olivine and clinopyroxene do not contain H_2O , hence the remaining magma becomes richer in H_2O content. In the study area, the pyroclastic sequence of the Eocene Alibaba Formation starts with the hornblende-poor basaltic-andesitic agglomerates and grades upward hornblende-rich andesitic agglomerates and volcanic breccias. This systematically increasing of hornblende content in the rocks from bottom to top within the sequence also strongly supports that the fractional crystallization was an important process during the petrogenetic evolution of the Kale non-adakitic magmas. In addition, the hornblende-rich porphyritic andesites (Pirahmet andesite), have very similar petrographic characteristics and trace-rare earth element distribution patterns to those of hornblende-rich lithologies consisting of the upper part of the non-adakitic pyroclastic sequence (Fig. 8C, D), suggesting that they were possibly derived from same magma source. It is clear that the eastern Pontides orogenic belt is a continental arc and its crustal thickness was at least 20–25 km in the early Eocene (Bektaş et al., 1995, 1999; Eyuboglu et al., 2006, 2007, 2011a). Therefore, the Kale non-adakitic magmas may have been affected by the crustal assimilation/contamination during their passage through the eastern Pontides arc crust to reach the surface. On the primitive mantle-normalized trace element distribution diagram, the existence of pronounced negative Nb-Ta anomalies and high abundance of Pb in the studied rocks indicate a subduction signature and a small amount of upper-crustal assimilation for the origin of the Kale non-adakitic magmas. However, the best evidence of assimilation/contamination comes from studies of radiogenic isotopes. According to Kaygusuz et al. (2011) the isotopic

compositions of Eocene calc-alkaline Torul volcanics, which are exposed at the 35 km northwest of the study area, are consistent with the subduction-induced sources and fractional crystallization rather than crustal assimilation. Similarly, Temizel and Arslan (2008) suggested that the eastern Pontides Tertiary volcanic rocks were modified by mainly fractional crystallization and minor assimilation processes. As a result, in comparison with fractional crystallization, crustal assimilation seems to have been a less important factor in genesis of early Eocene Kale non-adakitic magmas.

5.3. The nature of the transition from adakitic to non-adakitic magmatism

5.3.1. Geological and geochronological implications

In the study area, the adakitic lithologies can be divided into two main groups as porphyries and hyaloclastites. The adakitic porphyries exposed along an approximately NW–SE-trending zone in the study area occur as small, rounded or ellipsoidal intrusions within the autochthonous units of the eastern Pontides orogenic belt (Figs. 3 and 11A). They can be grouped into three subgroups as biotite-rich andesites (Kizil Tepe andesite), hornblende-rich andesite (Karakise Tepe andesite) and dacite (Kırcaova dacite) based on their petrographical characteristics. The zircon U–Pb dating on biotite-rich adakitic andesite indicates an age of 48.71 ± 0.74 Ma (late Ypresian–early Lutetian on the timescale of Gradstein et al. (2004)). The andesitic hyaloclastites represent the final stage of the adakitic activity in the Kale area. The adakitic magmatism was followed by an intense non-adakitic basaltic-andesitic magmatism in the study area. Immediately east of the Kale village is one of the best locations to view the transition from adakitic to non-adakitic magmatism in the southern part of the eastern Pontides orogenic belt (Figs. 3, 4D and 11). In this location, the late Cretaceous sediments are covered by a debris flow level including biotite-rich adakitic andesite fragments (Fig. 11B). The flow layer is ca. 14 m thick and exhibits a bedded structure. The fragments range from a few mm to 80 cm in size and are cemented by a nummulite-bearing sedimentary material, indicating that they accumulated in a shallow water environment. This level grades upward thick-bedded, gray-beige colored, nummulite and locally biotite-rich adakitic andesite fragments-bearing sandy limestone with about 2 m thickness (Fig. 11C). In addition, the existence of neptunian dikes (sedimentary dikes) filled by nummulite-bearing sandy limestone in the study area indicates an evidence for extensional tectonic regime during the Lutetian in the region (Eyuboglu, unpublished data). The nummulite-bearing limestone level is overlain by the andesitic hyaloclastite breccia representing the final stage of the adakitic activity in the Kale area (Fig. 11D). The thickness is about 24 m and features like sorting, preferential clast alignment or conspicuous bedding are absent. This monomict breccia display jigsaw-fit texture typical of in situ hyaloclastite (Fig. 11D). A fine-grained, dark red colored, sedimentary and fossiliferous matrix fills spaces between the hornblende-rich andesite clasts ranging from a few mm to 50 mm in size. These field observations indicate that the eruption/intrusion of adakitic andesitic magma into soft carbonate mud on a carbonate shelf generated this unit in the early Lutetian. The adakitic hyaloclastite breccia is locally covered by thick-medium bedded, yellowish gray and beige colored and nummulite-bearing sandy limestone, sandstone, marl and minor tuffite alternation (Fig. 11E). After the accumulation of this unit, an intense non-adakitic basaltic-andesitic magmatism started to erupt and as a result of this process, a thick pyroclastic sequence consisting mainly of calc-alkaline agglomerates and volcanic breccias were accumulated in the Kale area (Fig. 11F). Zircon U–Pb dating on hornblende-rich andesite taken from upper part of this pyroclastic sequence indicates an age

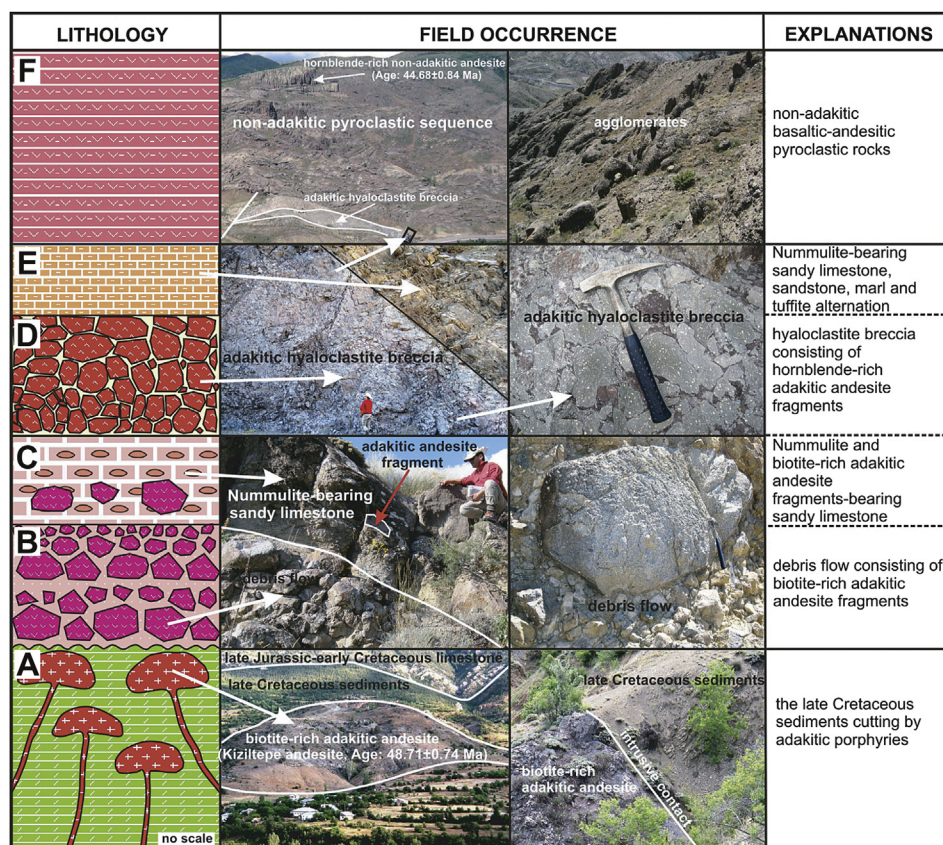


Figure 11. Detailed stratigraphic columnar section, showing the transition from adakitic to non-adakitic activity in the Kale area.

of 44.68 ± 0.84 Ma (Lutetian). Arslan and Aliyazıcıoğlu (2001) suggested that the volcanic activity in the Kale area started in the Paleocene and continued to the Eocene based on some fossil records obtained from the biotite-rich adakitic andesite fragments-bearing debris flow level (Fig. 11B). However, this study clearly indicates that the Cenozoic magmatism in the Kale area began with adakitic character in the late Ypresian–early Lutetian, not Paleocene and continued with non-adakitic character (Fig. 11).

5.3.2. Geodynamic and petrogenetic implications

The eastern Pontides orogenic belt is one of the best examples of long-term active continental margins in the world, where Tethys oceanic lithosphere is subducted beneath the Pontide continental lithosphere (e.g., Dewey et al., 1973; Bektaş et al., 1999; Eyuboglu et al., 2007, 2010, 2011a, 2012). According to Defant and Drummond (1990) the adakitic rocks in modern arc settings are produced by partial melting of a young (<25 Ma) and hot, subducting oceanic slab. In the following years, the studies on the thermal structure of subduction zones reveal that the adakitic melt generation is required to melting of very young oceanic crust (<5 Ma) and depths of about 25–90 km (Peacock et al., 1994; Peacock, 1996; Lopez and Castro, 2001). In this model, the melts generated at depths shallower 25 km produced non-adakitic granodioritic to tonalitic lithologies due to absence of the garnet in the restite. However, adakitic magmas reported from some settings such as slab window related to ridge subduction do not always confirm the thermal requirements associated subduction of very young oceanic crust (Thorkelson, 1996; Kinoshita, 2002; Thorkelson and Breitsprecher, 2005; Rodriguez et al., 2007; Zhang et al., 2010). Thorkelson and Breitsprecher (2005) suggested that the non-adakitic melts of granodioritic to tonalitic composition can form along the plate edges

at depths of 5–65 km, whereas adakitic melts form proximal to the plate edges at depths of 25–90 km in a slab window setting. In the active continental margins, the slab window formation and inflow of hot asthenosphere beneath subducted slab into mantle wedge triggers regional changes to mantle flow patterns, behavior of subducting plates, and characteristics of overlying lithosphere (Thorkelson, 1996). In these regions, the slab window-related magmatism can be generated by various processes such as heating of mantle wedge, mixing between sub-slab and supra-slab mantle reservoirs, partial melting of the subducted plate edges and extension in the overriding plate (Thorkelson, 1996). Our recent geological, geochemical and geochronological studies on the late Mesozoic–Cenozoic magmatism in the whole region indicates that a slab window formation related to ridge subduction and simultaneously slab roll-back processes started beneath the eastern Pontides magmatic arc in the late Paleocene and continued until the collision between Lesser Caucasus and greater Caucasus in the Oligo-Miocene (Eyuboglu et al., 2011a,b,c,d,e, 2012). The early Cenozoic adakitic activity started in the late Paleocene (~ 56 Ma) around Kop Mountain–Erzincan line in the far south of the eastern Pontides orogenic belt, migrated toward north in time, and ended in the early Eocene, at ~ 46 Ma, immediately north of the Torul–Bayburt–Ispir line (Eyuboglu et al., 2011a,b,c,d,e). To the north of this line, adakitic activity culminated the non-adakitic magmatism and continued to migrate toward trench (Fig. 12), supporting a slab window model as suggested by Thorkelson and Breitsprecher (2005).

The study area is located on the transition zone from adakitic magmatism to normal arc magmatism in the southern part of the eastern Pontides orogenic belt. In this area, the early Cenozoic magmatism is represented by two main cycles: adakitic (late Ypresian–early Lutetian) and non-adakitic magmatism (Lutetian).

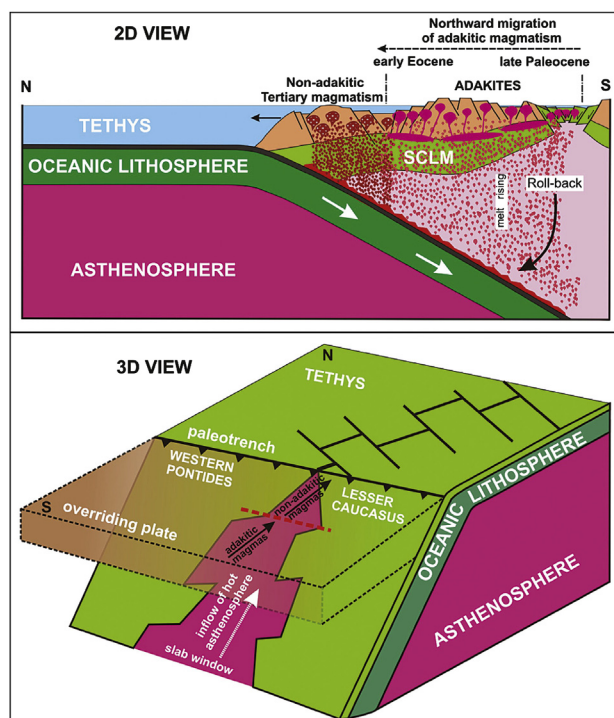


Figure 12. The geodynamic evolution model for the origin of the eastern Pontides early Cenozoic adakitic and non-adakitic magmas (modified from Eyuboglu et al., 2011a).

Our field observations and geochronological data indicate that there is no significant time gap during the transition from the adakitic to non-adakitic magmatism. The geochemical data indicate that both rock groups are LREE-enriched, with $(La/Yb)_N > 2$. When compared with the non-adakitic rocks, the adakitic rocks have higher values of the range of $(La/Yb)_N$ because of their low Yb contents and exhibit steeper REE patterns (Fig. 8B). The high $(La/Yb)_N$ corresponds to deeper melting leaving garnet-rich residues, while low $(La/Yb)_N$ magmas were separated from garnet-poor residues at shallower depth (Fig. 8A–D). All of the studied rocks are consistent with patterns expected for calc-alkaline rocks. The relative enrichment of Pb and Sr, at least, in both rock series, compared with primitive mantle, along with the relative depletion of Nb, Ta, and Ti, at least, shows that the magma source(s) were affected by subduction-related geochemical processes at some point in their history. Neither rock group shows pronounced Eu anomalies, nor are there other irregularities in the REE spectrum (Fig. 8B and D), indicating that there is a minimum role for plagioclase in controlling melting or fractionation, or the proportions of plagioclase to hornblende during fractionation are such that they cancel the Eu anomaly that normally would be related to plagioclase fractionation, or the patterns reflect mixing between magmas that have little Eu anomalies. In the studied rocks, the significant range of SiO_2 contents imply a dominant role either for fractional crystallization or for mixing between low- SiO_2 and high- SiO_2 magmas. There is overlap between the two groups in the overall abundance of rare earth elements, except for the HREE (Ho–Lu), where the highest concentrations in the adakites are still below the lowest concentrations in the non-adakites (Fig. 8B and D). There are two possibilities to explain this difference between both rock groups. The patterns could result from the same source by changing the degree of melting (higher degree of melting for the non-adakitic rocks), and changing the pressure at which melting is occurring (shallower for the non-adakitic rocks). The change of pressure might reflect

extension and thinning of the overlying crust, and upwelling of the source region. But the change in HREE content could also be due to a simple increase in the degree of melting at constant pressure until all garnet is effectively gone from the source. Thus, the low Y and low HREE signature that are characteristic of adakites disappear because garnet is no longer stable in the residue after melting. The second possibility is that the source of these two series of rocks is significantly different. The difference reflects, at the minimum, the stability of garnet in the source during the melting process; there may be other significant geochemical or mineralogical differences as well. Adakitic rocks have garnet \pm clinopyroxene \pm amphibole stable in the residue after melting, whereas the non-adakitic rocks formed in a source that did not contain significant garnet. This garnet-free source is at a shallower level in the mantle/crust. The progression from adakite to non-adakite reflects the advection of a thermal anomaly upward through the mantle/crust during the slab window formation, progressively causing melting at shallower levels. The suggestion that the non-adakitic rocks reflect higher degrees of melting implies that the shallower magma source is more “fertile”, in terms of being able to produce melt, than the deeper, adakitic, source.

6. Conclusions

- In the Kale area, the early Cenozoic magmatism is represented by two main cycles: adakitic and non-adakitic magmatism.
- The adakitic lithologies can be divided into two main groups as porphyries and hyaloclastites. The adakitic porphyries occur as small, rounded or ellipsoidal intrusions within the autochthonous units of the eastern Pontides orogenic belt. They can be grouped into three subgroups as biotite-rich andesite (Kizil Tepe andesite), hornblende-rich andesite (Karakise Tepe andesite) and dacite (Kircaova dacite) based on their petrographic characteristics. The hyaloclastites represent the final stage of adakitic activity in the study area and they were generated by eruption/intrusion of adakitic andesitic magma into soft carbonate mud.
- The non-adakitic lithologies include hornblende-rich porphyritic andesites (Pirahmet andesite) and a thick pyroclastic sequence consisting mainly of basaltic-andesitic agglomerates and volcanic breccias. All lithologies are cut by basaltic dikes of unknown age.
- Zircon U–Pb dating yielded ages of 48.71 ± 0.74 Ma (late Ypresian–early Lutetian) for the adakitic rocks, and 44.68 ± 0.84 Ma (Lutetian) for the non-adakitic magmatism, suggesting that there is no significant time gap during the transition from adakitic to non-adakitic magmatism.
- Both rock groups display enrichment in LIL and LRE elements relative to HFS and HRE elements, respectively, and also negative Nb, Ta and Ti anomalies, suggesting that magma(s) sources were affected by subduction-related geochemical processes at some point in their history.
- All the geological, geochemical and geochronological data indicate that the early Cenozoic Kale adakitic and non-adakitic magmas were generated by slab window processes related to ridge subduction in a south-dipping subduction zone, and not post-collisional setting. The data also suggest that the magma underwent fractional crystallization, mixing and contamination during their passage through the mantle and continental crust.

Acknowledgments

This study was supported by the Scientific and Technological Research Council of Turkey (TÜBİTAK, Grant No. 108Y309). Hasan

Basri DEMİR, İshak AY and Alparslan ŞEN are thanked for their assistance with fieldwork.

References

- Adamia, S.A., Lordkipanidze, M.B., Zakariadze, G.S., 1977. Evolution of an active continental margin as exemplified by the Alpine history of the Caucasus. *Tectonophysics* 40, 183–189.
- Arslan, M., Aliyazıcıoğlu, I., 2001. Geochemical and petrological characteristics of the Kale (Gumushane) volcanic rocks: implications for the Eocene evolution of eastern Pontide arc volcanism, Northeast Turkey. *International Geology Review* 43, 595–610.
- Arslan, M., Aslan, Z., 2006. Mineralogy, petrography and whole-rock geochemistry of the Tertiary Granitic Intrusions in the Eastern Pontides, Turkey. *Journal of Asian Earth Sciences* 27 (2), 177–193.
- Aslan, Z., 2010. U-Pb zircon SHRIMP age, geochemical and petrographical characteristics of tuffs within calc-alkaline Eocene volcanics around Gumushane (NE Turkey), Eastern Pontides. *Neues Jahrbuch Für Mineralogie* 187 (3), 329–346.
- Atherton, M.P., Petford, N., 1993. Generation of sodium-rich magmas from newly underplated basaltic crust. *Nature* 362, 144–146.
- Bektaş, O., Çapkinoglu, Ş., 1997. Doğu Pontid magmatik arkında (KD Türkiye) neptünien daykılar ve blok tektoniği. *Geosond* 30, 451–463.
- Bektaş, O., Yılmaz, C., Taslı, K., Akdağ, K., Özgür, S., 1995. Cretaceous rifting of the eastern Pontide carbonate platform (NE Turkey): the formation of carbonates breccias and turbidites as evidences of a drowned platform. *Geologia* 57 (1–2), 233–244.
- Bektaş, O., Şen, C., Atıcı, Y., Köprülü, N., 1999. Migration of the Upper Cretaceous subduction-related volcanism toward the back-arc basin of the eastern Pontide magmatic arc (NE Turkey). *Geological Journal* 34, 95–106.
- Bourdon, E., Eissen, J.P., Monzier, M., Robin, C., Martin, H., Cotton, J., Hall, M.L., 2002. Adakite-like lavas from Antisana volcano (Ecuador): evidence for slab melt metasomatism beneath the Andean volcanic zone. *Journal of Petrology* 43 (2), 199–217.
- Boynton, W.V., 1984. Cosmochemistry of rare earth elements: meteorite studies. In: Henderson, P. (Ed.), *Rare Earth Element Geochemistry*. Elsevier, Amsterdam, pp. 63–114.
- Casquet, C., Rapela, C.W., Pankhurst, R.J., Baldo, E., Galindo, C., Fanning, C.M., Dahlquist, J., 2012. Fast sediment underplating and essentially coeval juvenile magmatism in the Ordovician margin of Gondwana, Western Sierras Pampeanas, Argentina. *Gondwana Research* 22, 664–673.
- Castillo, P.R., Janney, P.E., Solidum, R.U., 1999. Petrology and geochemistry of Camiguin Island, southern Philippines: insights to the source of adakites and other lavas in a complex arc setting. *Contributions to Mineralogy and Petrology* 134, 33–51.
- Chiu, H.-Y., Chung, S.-L., Wu, F.-Y., Liu, D., Liang, Y.-H., Lin, I.J., Lizuka, Y., Xie, L.-W., Wang, Y., Chu, M.-F., 2009. Zircon U-Pb and Hf isotopic constraints from eastern Transhimalayan Batholiths on the postcollisional magmatic and tectonic evolution in southern Tibet. *Tectonophysics* 477, 3–19.
- Chung, S.L., Liu, D.Y., Ji, J.Q., Chu, M.F., Lee, H.Y., Wen, D.J., Lo, C.H., Lee, T.Y., Qian, Q., Zhang, Q., 2003. Adakites from continental collision zones: melting of thickened lower crust beneath southern Tibet. *Geology* 31, 1021–1024.
- Condie, K.C., 1993. Chemical composition and evolution of the upper continental crust: contrasting results from surface samples and shales. *Chemical Geology* 104, 1–37.
- Condie, K.C., 2005. TTGs and adakites: are they both slab melts? *Lithos* 80, 33–44.
- Condie, K.C., Kröner, A., 2012. The building blocks of continental crust: evidence for a major change in the tectonic setting of continental growth at the end of the Archean. *Gondwana Research*. <http://dx.doi.org/10.1016/j.gr.2011.09.011>.
- Defant, M.J., Drummond, M.S., 1990. Derivation of some modern arc magmas by melting of young subducted lithosphere. *Nature* 347, 662–665.
- Defant, M.J., Xu, J.F., Kepezhinskas, P., Wang, Q., Zhang, Q., Xiao, L., 2002. Adakites: some variations on a theme. *Acta Petrologica Sinica* 18, 129–142.
- Dewey, J.F., Pitman, W.C., Ryan, W.B.F., Bonnin, J., 1973. Plate tectonics and evolution of the Alpine system. *Geological Society of America Bulletin* 84, 3137–3180.
- Dilek, Y., İmamverdiyev, N., Altunkaynak, Ş., 2010. Geochemistry and tectonics of Cenozoic volcanism in the Lesser Caucasus (Azerbaijan) and the peri-Arabian region: collision-induced mantle dynamics and its magmatic fingerprint. *International Geology Review* 52 (4–6), 536–578.
- Dokuz, A., 2011. A slab detachment and delamination model for the generation of Carboniferous high-potassium I-type magmatism in the Eastern Pontides, NE Turkey: the Kose composite pluton. *Gondwana Research* 19 (4), 926–944.
- Eren, M., 1983. *trGümüshane-Kale arasındaki jeolojisi ve mikrofasiyes incelemesi*. Karadeniz Üniversitesi Fen Bilimleri Enstitüsü, MSc Thesis, p. 197.
- Eyuboglu, Y., 2010. Late Cretaceous high-K volcanism in the Eastern Pontide Orogenic Belt, and its implications for the geodynamic evolution of NE Turkey. *International Geology Review* 52 (2–3), 142–186.
- Eyuboglu, Y., Bektaş, O., Seren, A., Maden, N., Jacoby, W.R., Özer, R., 2006. Three axial extensional deformation and formation of the Liassic rift basins in the Eastern Pontides (NE Turkey). *Geologica Carpathica* 57 (5), 337–346.
- Eyuboglu, Y., Bektaş, O., Pul, D., 2007. Mid-Cretaceous olistostromal ophiolitic melange developed in the back-arc basin of the Eastern Pontide magmatic arc (NE Turkey). *International Geology Review* 49 (12), 1103–1126.
- Eyuboglu, Y., Dilek, Y., Bozkurt, E., Bektaş, O., Rojaj, B., Şen, C., 2010. Geochemistry and Geochronology of a reversely-zoned, Alaskan-type ultramafic–mafic complex in the Eastern Pontides, NE Turkey. In: Santosh, M., Maruyama, S. (Eds.), *A Tribute to Akiho Miyashiro*. Gondwana Research, 18, pp. 230–252.
- Eyuboglu, Y., Chung, S.L., Santosh, M., Dudas, F.O., Akaryali, E., 2011a. Transition from shoshonitic to adakitic magmatism in the Eastern Pontides, NE Turkey: implications for slab window melting. *Gondwana Research* 19, 413–429.
- Eyuboglu, Y., Santosh, M., Dudas, F.O., Chung, S.L., Akaryali, E., 2011b. Migrating magmatism in a continental arc: geodynamics of the Eastern Mediterranean revisited. *Journal of Geodynamics* 52, 2–15.
- Eyuboglu, Y., Santosh, M., Chung, S.L., 2011c. Crystal fractionation of adakitic magmas in the crust-mantle transition zone: petrology, geochemistry and U-Pb zircon chronology of the Seme adakites, Eastern Pontides, NE Turkey. *Lithos* 121, 151–166.
- Eyuboglu, Y., Santosh, M., Bektaş, O., Ayhan, S., 2011d. Arc magmatism as a window to plate kinematics and subduction polarity: example from the Eastern Pontides belt, NE Turkey. *Geoscience Frontiers* 2 (1), 49–56.
- Eyuboglu, Y., Santosh, M., Chung, S.L., 2011e. Petrochemistry and U-Pb ages of adakitic intrusions from the Pulur massif (Eastern Pontides, NE Turkey): implications for slab roll-back and ridge subduction associated with Cenozoic convergent tectonics in eastern Mediterranean. *Journal of Geology* 119, 394–417.
- Eyuboglu, Y., Santosh, M., Bektaş, O., Chung, S.L., 2011f. Late Triassic subduction-related ultramafic–mafic magmatism in the Amasya area (Eastern Pontides, NE Turkey): implications for the ophiolite conundrum in eastern Mediterranean. *Journal of Asian Earth Sciences* 42 (3), 234–257.
- Eyuboglu, Y., Santosh, M., Yi, K., Bektaş, O., Kwon, S., 2012. Discovery of Miocene adakitic dacite from the Eastern Pontides Belt and revised geodynamic model for the late Cenozoic evolution of eastern Mediterranean region. *Lithos* 146–147, 218–232.
- Feeley, T.C., Hacker, M.D., 1995. Intracrustal derivation of Na-rich andesitic and dacitic magmas – an example from volcan Ollague, Andean central volcanic zone. *Journal of Geology* 103 (2), 213–225.
- Gao, S., Rudnick, R.L., Yuan, H.L., Liu, X.M., Xu, W.L., Lin, W.L., Ayers, J., Wang, X.C., Wang, Q.H., 2004. Recycling lower continental crust in the North China Craton. *Nature* 432, 892–897.
- Gao, Y., Santosh, M., Hou, Z., Wei, R., Ma, G., Chen, Z., Wu, J., 2012. High Sr/Y magmas generated through crystal fractionation: evidence from Mesozoic volcanic rocks in the Northern Tianshan orogen, North China Craton. *Gondwana Research* 22, 152–168.
- Gradstein, F.M., Ogg, J.G., Smith, A.G., 2004. *A Geologic Time Scale 2004*. Cambridge University Press, Cambridge, p. 589.
- Guan, Q., Zhu, D.C., Zhao, Z.D., Dong, G.C., Zhang, L.L., Li, X.W., Liu, M., Mo, X.X., Liu, Y.S., Yuan, H.L., 2012. CRUSTAL thickening prior to 38 Ma in southern Tibet: evidence from lower crust-derived adakitic magmatism in the Gangdese Batholith. *Gondwana Research* 21, 88–99.
- Guo, F., Fan, W., Li, C., 2006. Geochemistry of late Mesozoic adakites from the Sulu belt, eastern China: magma genesis and implications for crustal recycling beneath continental collisional orogens. *Geological Magazine* 143 (1), 1–13.
- Gutscher, M.A., Maury, R., Eissen, J.P., Bourdon, E., 2000. Can slab melting be caused by flat subduction? *Geology* 28, 535–538.
- Güven, I.H., 1993. *Geological and Metallogenic Map of the Eastern Black Sea Region; 1:250000 Map*. MTA, Trabzon.
- Hastie, A.R., Kerr, A.C., Pearce, J.A., Mitchell, S.F., 2007. Classification of altered volcanic island arc rocks using immobile trace elements: development of the Th–Co discrimination diagram. *Journal of Petrology* 48 (12), 2341–2357.
- Johnson, K., Barnes, C.G., Miller, C.A., 1997. Petrology, geochemistry, and genesis of high-Al tonalite and trondhjemites of the Cornucopia stock, Blue Mountains, Northeastern Oregon. *Journal of Petrology* 38, 1585–1611.
- Karsli, O., Chen, B., Aydın, F., Şen, C., 2007. Geochemical and Sr–Nd–Pb isotopic compositions of the Eocene Dölek and Sarıçekirgen Plutons, Eastern Turkey: implications for magma interaction in the genesis of high-K calc-alkaline granitoids in a post-collision extensional setting. *Lithos* 98, 67–96.
- Karsli, O., Dokuz, A., Uysal, İ., Aydın, F., Kandemir, R., Wijbrans, R.J., 2010. Generation of the early Cenozoic adakitic volcanism by partial melting of mafic lower crust, Eastern Turkey: implications for crustal thickening to delamination. *Lithos* 114, 109–120.
- Kay, R.W., 1978. Aleutian magnesian andesites: melts from subducted Pacific ocean crust. *Journal of Volcanology and Geothermal Research* 4, 117–132.
- Kaygusuz, A., Siebel, W., Şen, C., Satır, M., 2008. Petrochemistry and petrology of I-type granitoids in an arc setting: the composite Torul Pluton, eastern Pontides, NE Turkey. *International Journal of Earth Sciences* 97, 739–764.
- Kaygusuz, A., Arslan, M., Siebel, W., Şen, C., 2011. Geochemical and Sr–Nd isotopic characteristics of post-collisional calc-alkaline volcanics in the eastern Pontides. *Turkish Journal of Earth Sciences* 20, 137–159.
- Kinoshita, O., 2002. Possible manifestations of slab window magmatism in Cretaceous southwest Japan. *Tectonophysics* 344, 1–13.
- Lagabriele, Y., Guivel, C., Maury, R.C., Bourgois, J., Fourcade, S., Martin, H., 2000. Magmatic–tectonic effects of high thermal regime at the site of active ridge subduction: the Chile triple junction model. *Tectonophysics* 326, 255–268.
- Le Bas, M.J., Le Maitre, R.W., Streckeisen, A., Zanettin, B., 1986. A chemical classification of volcanic rocks based on the total alkali–silica diagram. *Journal of Petrology* 27, 745–750.
- Lopez, S., Castro, A., 2001. Determination of the fluid-absent solidus and supersolidus phase relationships of MORB-derived amphibolites in the range 4–14 kbar. *American Mineralogist* 86, 1396–1413.
- Martin, H., 1998. Adakitic magmas: modern analogues of Archean granitoids. *Lithos* 46, 411–429.

- Martin, H., Smithies, R.H., Rapp, R., Moya, J.F., Champion, D., 2005. An overview of adakite, tonalite-trondhjemite-granodiorite (TTG), and sanukitoid: relationships and some implications for crustal evolution. *Lithos* 79, 1–24.
- Muir, R.J., Weaver, S.D., Bradshaw, J.D., Eby, G.N., Evans, J.A., 1995. Geochemistry of the Cretaceous Separation Point Batholith, New Zealand: granitoid magmas formed by melting of mafic lithosphere. *Journal of Geological Society London* 152, 689–701.
- Okay, A.I., Sahintürk, Ö., 1997. Geology of the Eastern Pontides. In: Robinson, A.G. (Ed.), *Regional and Petroleum Geology of the Black Sea and Surrounding Region*. Memoir, vol. 68. American Association of Petroleum Geologists, pp. 291–311.
- Peacock, S.M., 1996. Thermal and petrologic structure of subduction zones (overview). In: Bebout, G.E., Scholl, D.W., Kirby, S.H., Platt, J.P. (Eds.), *Subduction Top to Bottom*. Geophysical Monograph, vol. 96. American Geophysical Union, Washington, DC, pp. 119–133.
- Peacock, S.M., Rushmer, T., Thompson, A.B., 1994. Partial melting of subducting oceanic crust. *Earth and Planetary Science Letters* 121, 227–244.
- Petford, N., Atherton, M., 1996. Na-rich partial meltings from newly underplated basaltic crust: the Cordillera Blanca Batholith, Peru. *Journal of Petrology* 37, 1491–1521.
- Plank, T., Langmuir, C.H., 1998. The chemical composition of subducting sediment and its consequences for the crust and mantle. *Chemical Geology* 145, 325–394.
- Qi, X., Zeng, L., Zhu, L., Hu, Z., Hou, K., 2012. Zircon U-Pb and Lu-Hf isotopic systematics of the Daping plutonic rocks: implications for the Neoproterozoic tectonic evolution of the northeastern margin of the Indochina block, Southwest China. *Gondwana Research* 21, 180–193.
- Rapp, R.P., Shimizu, N., Norman, M.D., Applegate, G.S., 1999. Reaction between slab-derived melts and peridotite in the mantle wedge: experimental constraints at 3.8 GPa. *Chemical Geology* 160, 335–356.
- Rapp, R.P., Xiao, L., Shimizu, N., 2002. Experimental constraints on the origin of potassium-rich adakites in east China. *Acta Petrologica Sinica* 18, 293–311.
- Rickwood, P.C., 1989. Boundary lines within petrologic diagrams which use oxides of major and minor elements. *Lithos* 22, 247–263.
- Rodriguez, C., Selles, D., Dungan, M., Langmuir, C., Leeman, W., 2007. Adakitic dacites formed by intracrustal crystal fractionation of water-rich parent magmas at Nevado de Longavi Volcano (36.2°S, Andean Southern Volcanic Zone, Central Chile). *Journal of Petrology* 48 (11), 2033–2061.
- Rubatto, D., 2002. Zircon trace element geochemistry: partitioning with garnet and the link between U-Pb ages and metamorphism. *Chemical Geology* 184, 23–138.
- Sajona, F.G., Maury, R.C., Bellon, H., Cotten, J., Defant, M.J., Pubellier, M., Rangin, C., 1993. Initiation of subduction and the generation of slab melts in western and eastern Mindanao, Philippines. *Geology* 21, 1007–1010.
- Santosh, M., Kusky, T., 2010. Origin of paired high pressure-ultrahigh-temperature orogens: a ridge subduction and slab window model. *Terra Nova* 22 (1), 35–42.
- Santosh, M., Maruyama, S., Sato, K., 2009. Anatomy of a Cambrian suture in Gondwana: Pacific type orogeny in southern India? *Gondwana Research* 16 (2), 321–341.
- Şengör, A.M.C., Yılmaz, Y., 1981. Tethyan evolution of Turkey: a plate tectonic approach. *Tectonophysics* 75, 181–241.
- Shimoda, G., Tatsumi, Y., Nohda, S., Ishizaka, K., Jahn, B.M., 1998. Setouchi high-Mg andesites revisited: geochemical evidence for melting of subducting sediments. *Earth and Planetary Science Letters* 160, 479–492.
- Stern, C.R., Kilian, R., 1996. Role of the subducted slab, mantle wedge and continental crust in the generation of adakites from the Austral Volcanic Zone. *Contributions to Mineralogy and Petrology* 123, 263–281.
- Sun, S.S., McDonough, W.F., 1989. Chemical and isotopic systematics of ocean basalts: implications for mantle composition and process. In: Saunders, A.D., Norry, M.J. (Eds.), *Magmatism in the Ocean Basins*. Geological Society of London, vol. 42, pp. 313–345.
- Temizel, I., Arslan, M., 2008. Petrology and geochemistry of Tertiary volcanic rocks from the İkizce (Ordu) area, NE Turkey: implications for the evolution of the eastern Pontide paleo-magmatic arc. *Journal of Asian Earth Sciences* 31 (4–6), 439–463.
- Thorkelson, D.J., 1996. Subduction of diverging plates and the principles of slab window formation. *Tectonophysics* 255, 47–63.
- Thorkelson, D.J., Breitsprecher, K., 2005. Partial melting of slab window margins: genesis of adakitic and non-adakitic magmas. *Lithos* 79, 25–41.
- Topuz, G., Altherr, R., Schwarz, W.H., Dokuz, A., Meyer, H.P., 2007. Variscan amphibolite-facies rocks from the Kurtoglu metamorphic complex (Gumushane area, Eastern Pontides, Turkey). *International Journal of Earth Sciences* 96 (5), 861–873.
- Topuz, G., Altherr, R., Siebel, W., Schwarz, W.H., Zack, T., Hasozbek, A., Barth, M., Satir, M., Sen, C., 2010. Carboniferous high-potassium I-type granitoid magmatism in the Eastern Pontides: the Gumushane pluton (NE Turkey). *Lithos* 116 (1–2), 92–110.
- Topuz, G., Okay, A.I., Altherr, R., Schwarz, W.H., Siebel, W., Zack, T., Satir, M., Şen, C., 2011. Post-collisional adakite-like magmatism in the Ağvanis Massif and implications for the evolution of the Eocene magmatism in the Eastern Pontides (NE Turkey). *Lithos* 125 (1–2), 131–150.
- Ustaömer, T., Robertson, A.H.F., 1996. Paleotethyan tectonic evolution of the North Tethyan margin in the central Pontides, N Turkey. In: Erler, A., Ercan, T., Bingöl, E., Örcen, S. (Eds.), *International Symposium on the Geology of the Black Sea Region*, Proceedings-I, pp. 24–33.
- Wang, Q., Xu, J.F., Zhao, Z.H., Bao, Z.W., Xu, W., Xiong, X.L., 2004. Cretaceous high-potassium intrusive rocks in the Yueshan-Hongzhen area of east China: adakites in an extensional tectonic regime within a continent. *Geochemical Journal* 38, 417–434.
- Wang, Q., McDermott, F., Xu, J.F., Bellon, H., Zhu, Y.T., 2005. Cenozoic K-rich adakitic volcanic rocks in the Hohxil area, northern Tibet: lower crustal melting in an intracontinental setting. *Geology* 33, 464–468.
- Wang, Q., Derek, A.W., Xu, J.F., Zhao, Z.H., Jian, P., Xiong, X.L., Bao, Z.W., Li, C.F., Bai, Z.H., 2006a. Petrogenesis of Cretaceous adakitic and shoshonitic igneous rocks in the Luzong area, Anhui Province (eastern China): implications for geodynamics and Cu-Au mineralizations. *Lithos* 89, 424–446.
- Wang, Q., Xu, J.F., Jian, P., Bao, Z.W., Zhao, Z.H., Li, C.F., Xiong, X.L., Ma, J.L., 2006b. Petrogenesis of adakitic porphyries in an extensional tectonic setting, Dexing, South China: implications for the genesis of porphyry copper mineralization. *Journal of Petrology* 47, 119–144.
- Xu, J.F., Shinjio, R., Defant, M.J., Wang, Q., Rapp, R.P., 2002. Origin of Mesozoic adakitic intrusive rocks in the Ningzhen area of east China: partial melting of delaminated lower continental crust? *Geology* 30, 1111–1114.
- Zhang, Z., Zhao, G., Santosh, M., Wang, J., Dong, X., Shen, K., 2010. Late Cretaceous charnockite with adakitic affinities from the Gangdese batholith, southeastern Tibet: evidence for Neo-Tethyan mid-ocean ridge subduction? *Gondwana Research* 17 (4), 615–631.